Citation: Molecular Therapy–Nucleic Acids (2012) 1, e22; doi:10.1038/mtna.2012.16

www.nature.com/mtna

Cholesterol-lowering Action of BNA-based Antisense Oligonucleotides Targeting PCSK9 in Atherogenic Diet-induced Hypercholesterolemic Mice

Tsuyoshi Yamamoto[1,2], Mariko Harada-Shiba[2], Moeka Nakatani[1,2], Shunsuke Wada[2,3], Hidenori Yasuhara[1,2], Keisuke Narukawa[1], Kiyomi Sasaki[3], Masa-Aki Shibata[4], Hidetaka Torigoe[3], Tetsuji Yamaoka[5], Takeshi Imanishi[6] and Satoshi Obika[1]

Recent findings in molecular biology implicate the involvement of proprotein convertase subtilisin/kexin type 9 (PCSK9) in low-density lipoprotein receptor (LDLR) protein regulation. The cholesterol-lowering potential of anti-PCSK9 antisense oligonucleotides (AONs) modified with bridged nucleic acids (BNA-AONs) including 2′,4′-BNA (also called as locked nucleic acid (LNA)) and 2′,4′-BNA^{NC} chemistries were demonstrated both *in vitro* and *in vivo*. An *in vitro* transfection study revealed that all of the BNA-AONs induce dose-dependent reductions in PCSK9 messenger RNA (mRNA) levels concomitantly with increases in LDLR protein levels. BNA-AONs were administered to atherogenic diet-fed C57BL/6J mice twice weekly for 6 weeks; 2′,4′-BNA-AON that targeted murine PCSK9 induced a dose-dependent reduction in hepatic PCSK9 mRNA and LDL cholesterol (LDL-C); the 43% reduction of serum LDL-C was achieved at a dose of 20 mg/kg/injection with only moderate increases in toxicological indicators. In addition, the serum high-density lipoprotein cholesterol (HDL-C) levels increased. These results support antisense inhibition of PCSK9 as a potential therapeutic approach. When compared with 2′,4′-BNA-AON, 2′,4′-BNA^{NC}-AON showed an earlier LDL-C–lowering effect and was more tolerable in mice. Our results validate the optimization of 2′,4′-BNA^{NC}-based anti-PCSK9 antisense molecules to produce a promising therapeutic agent for the treatment of hypercholesterolemia.

Molecular Therapy–Nucleic Acids (2012) **1**, e22; doi:10.1038/mtna.2012.16; published online 15 May 2012

Introduction

Statins are lipid-lowering drugs that achieve a strong reduction of serum low-density lipoprotein cholesterol (LDL-C) mainly *via* the indirect activation of LDL receptor (LDLR)-mediated hepatic uptake of LDL from the blood.[1,2] The development of drugs that directly regulate the expression of hepatic LDLR would thus be a compelling strategy to obtain the efficacy of statin-induced LDL-C reduction while compensating for potential weaknesses of statin therapy, such as severe adverse effects (e.g., myopathy). The molecular basis of LDLR regulation as well as cholesterol maintenance has been enthusiastically elucidated,[2–7] and several causative molecules of hypercholesterolemia relevant to the direct regulation of LDLR function have recently been identified.[8–11] Proprotein convertase subtilisin/kexin type 9 (PCSK9), which was recently identified as the third gene relevant to autosomal dominant hypercholesterolemia,[10] is involved in the maintenance of cholesterol balance. A number of human mutations in PCSK9 have been reported. Gain-of-function mutations are associated with autosomal dominant hypercholesterolemia, whereas loss-of-function mutations are relevant to low blood levels of LDL-C.[12] Recent findings have suggested the involvement of PCSK9 in LDLR regulation. PCSK9 is synthesized mainly in the liver, small intestine, and kidney as a 72-kDa soluble zymogen that subsequently undergoes autocatalytic cleavage into an active form. The active 63-kDa enzyme in complex with the cleaved prodomain is secreted into the bloodstream. Secreted PCSK9 directly binds to an extracellular part of the LDLR. The LDLR–PCSK9 complex is transported from the cell surface to the endosomal system for digestion. PCSK9 forms a stable complex with LDLR in lysosomes, which disturbs the recycling of LDLR to reduce LDL uptake.[4,13,14] PCSK9 would be a pivotal regulator of LDLR and an attractive target for lipid-lowering therapy, although some molecular functions of PCSK9 remain unknown.

To achieve PCSK9 inhibition, several "molecular-targeted" approaches have been attempted. To our knowledge, berberine, an isoquinoline plant alkaloid, is the sole small molecule that achieves suppression of PCSK9 expression at the transcriptional level.[15–17] An antibody against secreted PCSK9 efficiently reduced the serum LDL-C levels of mice and monkeys.[18] Small interfering RNA formulated in a lipidoid nanoparticle can induce liver-specific reduction of PCSK9 messenger RNA (mRNA) and serum total cholesterol levels in wild-type mice.[19] These proof-of-concept studies demonstrate the therapeutic promise of PCSK9-targeted therapies. Antisense inhibition of PCSK9 is superior to the aforementioned strategies because antisense oligonucleotide (AON) molecules can deactivate intrahepatic mRNA as well as proteins in the blood; in addition, they target the liver *via* a simple delivery methodology. Graham *et al.* showed that 2′-*O*-methoxyethyl-modified phosphorothioate oligonucleotide (MOE) (100 mg/kg/week) administered for a 6-week period to mice fed a high-fat diet reduced hepatic

[1]Graduate School of Pharmaceutical Sciences, Osaka University, Suita, Japan; [2]Department of Molecular Innovation in Lipidology, National Cerebral and Cardiovascular Center Research Institute, Suita, Japan; [3]Faculty of Science, Tokyo University of Science, Shinjuku-ku, Japan; [4]Faculty of Health Science, Osaka Health Science University, Osaka, Japan; [5]Department of Biomedical Engineering, National Cerebral and Cardiovascular Center Research Institute, Suita, Japan; [6]BNA Inc., Ibaraki, Japan
Correspondence: Satoshi Obika, 1-6 Yamadaoka, Suita, Osaka 565-0871, Japan. E-mail: obika@phs.osaka-u.ac.jpor Mariko Harada-Shiba, 5-7-1 Fujishirodai, Suita, Osaka 565-8565, Japan. E-mail: shiba.mariko.ri@mail.ncvc.go.jp

Received 6 November 2011; revised 10 April 2012; accepted 10 April 2012

Keywords: antisense; BNA; hypercholesterolemia; LNA; PCSK9

PCSK9 mRNA and serum LDL-C. However, a large dose of MOE is necessary to obtain sufficient efficacy. More recently, Gupta *et al.* demonstrated that a reduced amount of 2′,4′-bridged nucleic acid (BNA) (also called as locked nucleic acid (LNA))-modified gapmer efficiently suppresses PCSK9 mRNA and induces an increase in LDLR protein levels both *in vitro* and *in vivo*.[20] Due to the high-affinity binding of 2′,4′-BNA–modified AON molecules, in many cases, 2′,4′-BNA–modified gapmer shows improved antisense potency *in vivo* as compared to MOE-based gapmer. However, in some cases, the repeated administration of 2′,4′-BNA–modified gapmer causes hepatotoxicity.[21] The development of more potent and less toxic antisense molecules is necessary for clinical usage.[22] We have developed a series of 2′,4′-BNAs such as 2′,4′-BNA and 2′,4′-BNA^{NC}, which have chemical bridges between the 2′ and 4′ positions of the ribose rings; 2′,4′-BNA^{NC}–modified oligonucleotides retain high-affinity binding to RNA and higher nuclease stability than 2′,4′-BNA–modified oligonucleotides.[23–25] Therefore, 2′,4′-BNA^{NC}–modified anti-PCSK9 AONs would be expected to possess distinct cholesterol-lowering potency and toxicological risks *in vivo*. Actually, 2′,4′-BNA^{NC}–modified phosphatase and tensin homolog deleted from chromosome ten (PTEN) inhibitor showed high potency without the onset of hepatotoxicity.[26] In this study, we present the effective gene silencing and cholesterol-lowering effects of both 2′,4′-BNA– and 2′,4′-BNA^{NC}–based anti-PCSK9 AON. In addition, we showed the toxicological characteristics of 2′,4′-BNA– and 2′,4′-BNA^{NC}–based AONs.

Results

Physicochemical properties of a 2′,4′-BNA–modified anti-PCSK9 AON *in vitro*

The 2′,4′-BNA–modified phosphorothioate oligonucleotides (P900SL) and a conventional phosphorothioate AON (P900S) were designed based on the previously identified potential sequence.[27] The control sequence was CR01S, which has the same conventional phosphorothioate backbone as P900S, but does not target any specific genes in mice (**Table 1**). Upper and lower case letters in the sequences represent 2′,4′-BNA and DNA, respectively. We additionally selected another sequence, a consensus sequence between the mouse and human sequences to dispense with the sequence translation to adapt to human clinical trials. P901SL and P901SNC both possess five gaps, and nine of 20 nucleotides are substituted by 2′,4′-BNA and 2′,4′-BNA^{NC} (**Table 1**, **Figure 1**). Note that the sequence, length, and composition of AONs have not been fully optimized yet here. The melting temperature (T_m) values of P900S, P900SL, P901S, P901SL, and P901SNC with their target RNA were determined by UV-melting experiments. AONs modified with 2′,4′-BNA and 2′,4′-BNA^{NC} showed an excellent target affinity compared to conventional phosphorothioate AONs (**Table 1**).

In vitro gene silencing properties

We next evaluated *in vitro* gene silencing properties of AONs by using mice hepatic NMuLi cells (**Figure 2a–c**) treated with 1–50 nmol/l of P900SL by means of lipofection. Real-time reverse transcription-PCR revealed a dose-dependent reduction of the PCSK9 mRNA level as compared to the GAPDH mRNA level (half-maximal inhibitory concentration (IC_{50}) = 3.0 nmol/l) (**Figure 2a**). By contrast, no such effective reduction of the mRNA level occurred in P900S-treated cells (IC_{50} = 41.2 nmol/l) (**Figure 2a**), and treatment with CR01S and CR01SL did not yield any silencing (**Figure 2b**). To investigate whether suppression of PCSK9 mRNA by P900SL affects the PCSK9 protein level, we performed western blotting experiments. A dose-dependent reduction of the PCSK9 protein level occurred in P900SL-treated NMuLi cells (**Figure 2a**). On the other hand, the protein levels of LDLR in P900SL-treated cells were increased in a dose-dependent manner, showing the inverse relationship between PCSK9 and LDLR protein levels. PCSK9 protein was thoroughly inhibited by P900SL at a concentration of ~10 nmol/l. The increase in LDLR protein simultaneously reached a plateau at this concentration. Gene silencing properties of P901S, P901SL, and P901SNC were demonstrated both in murine and human hepatic cell lines. P901SL and P901SNC showed a similar silencing efficacy as P900SL in NMuLi cells (**Figure 2a**). Both P901SL and P901SNC showed far more efficient mRNA inhibitory activity than P901S in HepG2 cells (**Figure 2d**). The reduction rate of PCSK9 protein levels also supported this trend (**Figure 2e**).

Table 1 Properties of modified oligonucleotides used in this study

Sequence ID	Sequence[a]	T_m	IC_{50} (nmol/l)	
			NMuLi	HepG2
CR01S	5′-ccttccctgaaggttcctcc-3′	–	N.D.	–
CR01SL	5′-cctTCCctgaagGTTCcTCc-3′	–	N.D.	–
P900S	5′-gggctcatagcacattatcc-3′	37.0	23	–
P900SL	5′-GggCTCatagcaCaTTaTCc-3′	72.1	1.8	–
P901S	5′-ccaggcctatgagggtgccg-3′	49.6	–	100
P901SL	5′-CCaggCCTaTgagggTgCCg-3′	83.2	1.0	1.8
P901SNC	5′-CCaggCCTaTgagggTgCCg-3′	86.0	3.0	11.6

Abbreviations: BNA, bridged nucleic acid; IC_{50}, half-maximal inhibitory concentration.
[a]Oligonucleotides with 2′,4′-BNA (upper case), 2′,4′-BNA^{NC} (capital italic), and DNA (lower case letters). All internucleotide linkages are phosphorothioated. Melting temperature (T_m) of CR01S and CR01SL were not measured because no target site on transcripts, marked "–". Non-detectable IC_{50} values, due to low potency, marked N.D. IC_{50} values were partly not determined, marked "–".

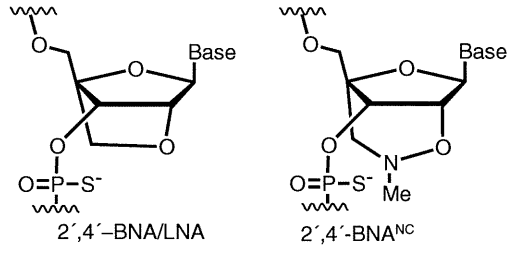

Figure 1 Structure of bridged nucleic acids (BNA) used in this study. LNA, locked nucleic acid.

The level of intrahepatic AONs in normal chow-fed mice after a single treatment with BNA-modified AONs

Next, we examined whether BNA-modified AONs can also be good inhibitors of PCSK9 in mice. A naked AON (P900SL) was intravenously (i.v.), subcutaneously (s.c.), and

intraperitoneally (i.p.) injected into normal chow-fed C57BL/6J mice (**Figure 3**). After 72 hours, the hepatic PCSK9 mRNA levels were measured, and the half-maximal effective dose (ED_{50}) values were determined. Intravenous administration showed the most efficient hepatic reduction of PCSK9 mRNA (ED_{50} = 7.5 mg/kg) (**Figure 3a**). Subcutaneous and intraperitoneal injections resulted in ED_{50} values of 8.8 and 12.1 mg/kg, respectively (**Figure 3c,d**). Next, we measured the amount of intact P900SL that accumulated in the liver after i.v. administration by using a previously described ELISA method.[28] The intrahepatic content of P900SL was directly proportional to the applied doses, and the saturation of accumulation was not observed even at the highest dose of 70 mg/kg, which is consistent with a previous report[29] (**Figure 3b**).

Repeated administration of BNA-modified AONs to atherogenic diet-fed mice

To determine the pharmacological effects of BNA-modified AONs, we monitored the serum cholesterol change upon repeated administration of AONs. Naked AONs (P900S and P900SL) were i.p. injected into atherogenic diet (cholesterol content, 1.25%)-fed C57BL/6J mice twice during 5 days at a dosage of 10 mg/kg per administration. Injections were performed on days 1 and 4. On day 5, livers were harvested to measure gene expression, and blood was collected for the lipid component analysis and toxicity evaluation. As shown in **Figure 4a,** a significant silencing effect of the hepatic PCSK9 mRNA level was only observed in the P900SL-treated arm. The increase in hepatic LDLR protein was shown by western blotting analysis (**Figure 4c**). The average serum LDL-C levels were concomitantly reduced by ~30%, although no statistically significant differences were observed (**Figure 4b**). Collectively, P900SL showed a mild cholesterol-lowering effect in this short-term experiment with the lack of serum elevation of liver transaminases, aspartate aminotransferase and alanine aminotransferase (ALT) (**Figure 4d**).

To obtain cholesterol-lowering efficacy profiles and toxicological information, we next performed longer-term and multiple-dose experiments in mice. P900SL was i.p. injected twice weekly at a dosage of 2–40 mg/kg/week for 6 weeks into high-cholesterol–loaded mice. After 4 weeks of treatment, blood samples were collected from tail veins, and the precise cholesterol profiles in serum lipoproteins were analyzed by the high-performance liquid chromatography method. **Supplementary Table S1** shows the raw serum total cholesterol levels and the cholesterol levels of fractionated lipoprotein components. **Figure 5a,b** show raw data plots of the high-performance liquid chromatography analysis of serum and the serum LDL-C ratio. Total cholesterol levels did not show a cholesterol-lowering effect or any other specific trends with an increase of doses. However, a precise lipoprotein component analysis revealed that P900SL had induced a dose-dependent LDL-C reduction, and the serum LDL-C reduction of 43% was achieved at a dose of 40 mg/kg/week, whereas serum HDL-C levels increased inversely with LDL-C levels. After a 6-week dosing regimen, livers and blood were harvested to analyze gene and protein expression and toxicities. A dose-dependent decrease of LDL-C, as seen at week 4, was continuously observed. Intrahepatic cholesterol content showed no significant difference between arms (**Supplementary Figure S1 and Supplementary Materials and Methods**). Hepatic gene expression levels were analyzed by the real-time reverse transcription-PCR method. Hepatic PCSK9 mRNA was efficiently reduced in a dose-dependent manner (**Figure 5c**). And, the reduction of PCSK9 mRNA did not affect LDLR mRNA expression levels (**Figure 5e**). However, LDLR protein levels increased concomitantly with decreased LDL-C levels (**Figure 5d**). Hepatic LDLR protein levels were significantly increased by ~1.5-fold in a dose-dependent manner. Note that we here collected sera and analyzed lipid profiles 2 weeks ahead of sacrifice in order to distribute the stressors associated with treatments, which strongly disturbs serum cholesterol levels.

Related gene expression associated with repeated dosing

We further investigated the effect of BNA-modified AONs on molecules related to the cholesterol metabolism (**Figure 5e**). Knockdown of PCSK9 mRNA induced a reduction in the gene expression of sterol regulatory element-binding protein 2 (SREBP2), a transcriptional factor controlling sterol synthesis; hydroxymethylglutaryl-CoA (HMG-CoA) synthase, an enzyme in the cholesterol synthesis pathway; hepatic triglyceride lipase (LIPC); and ATP-binding cassette transporter (ABCA1), a key enzyme for HDL production. On the other hand, scavenger receptor class B type 1 (SR-B1), a receptor for HDL particles, and cholesterol acyltransferase (ACAT1) showed no significant change, and the expression level of cholesterol 7α-hydroxylase (CYP7A1), the first and rate-limiting enzyme in bile acid synthesis, dose-dependently increased.

Toxicological characteristics of BNA-AONs associated with repeated dosing

Toxicological characteristics of P900SL upon subchronic dosing were estimated by an analysis of blood biochemistry and a histopathological analysis (**Figure 6**). Because phosphorothioate AONs accumulate mainly in the kidney and liver,[30–32] hepatotoxicity and renal toxicity are the most likely types of toxicity; 2′,4′-BNA–based AONs have the potential to induce hepatotoxicity.[21] However, our experiments showed only moderate increases in liver transaminases (even at higher doses of P900SL) and a dose-dependent mild increase in serum blood urea nitrogen levels (**Figure 6a**). Histopathologically, no treatment-related changes were seen in the liver or kidneys. As shown in **Figure 6b**, although the majority of mice treated with saline or therapeutic regimes showed cloudy swelling of hepatocytes, no cellular damage was found in the centrilobular and perilobular hepatocytes, which frequently experience toxicological insults. In addition, granulomas or inflammation were sporadically observed in the saline group and treated groups (**Supplementary Table S2**).

Repeated administration of 2′,4′-BNA^{NC}–modified AONs to atherogenic diet-fed mice with the least toxicity

To examine the effect of 2′,4′-BNA^{NC}–modified AONs, P901SNC as well as P901SL were applied to atherogenic diet-fed mice to investigate their potencies and toxicity profiles. P901SL and P901SNC were i.p. administered twice weekly for 6 weeks at a dose of 1–20 and 1–10 mg/kg/injection, respectively. On week 4, peripheral blood was collected from tail veins, and

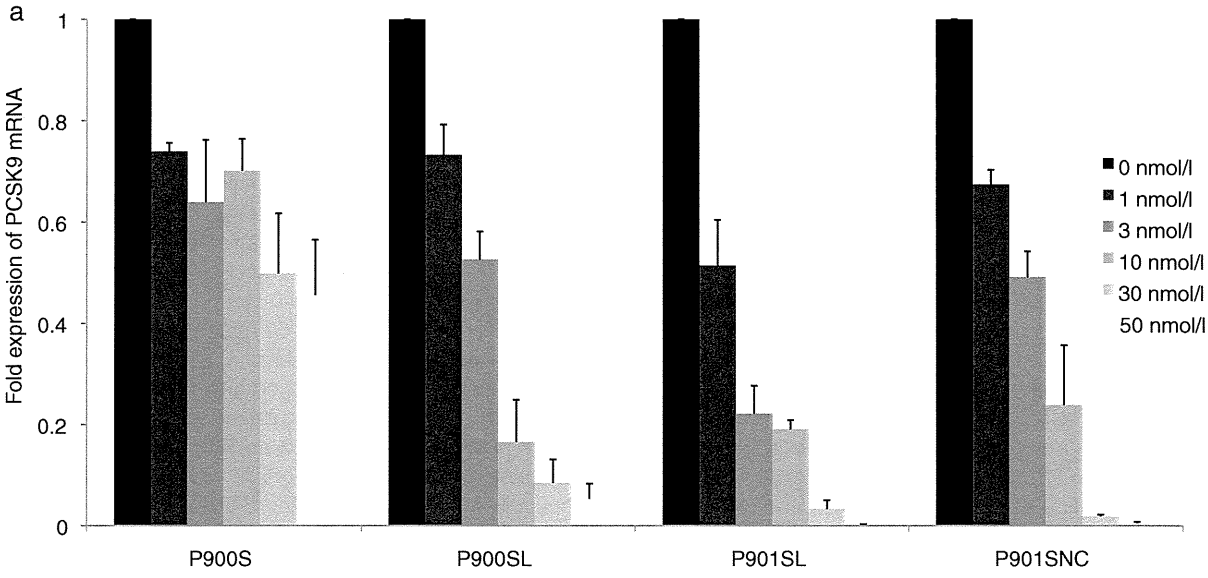
a
Fold expression of PCSK9 mRNA
1
0.8
0.6
0.4
0.2
0
P900S
P900SL
P901SL
P901SNC
0 nmol/l
1 nmol/l
3 nmol/l
10 nmol/l
30 nmol/l
50 nmol/l

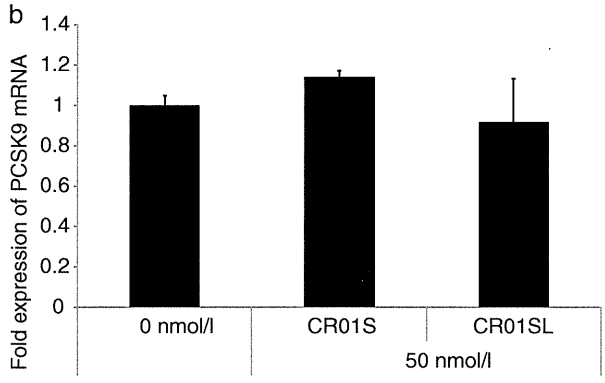
b
Fold expression of PCSK9 mRNA
1.4
1.2
1
0.8
0.6
0.4
0.2
0
0 nmol/l
CR01S
CR01SL
50 nmol/l

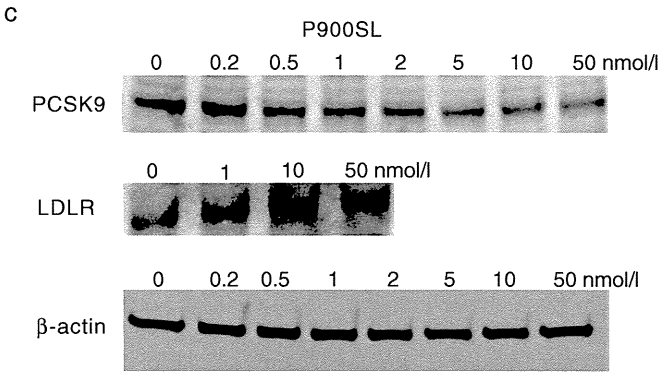
c
P900SL
0 0.2 0.5 1 2 5 10 50 nmol/l
PCSK9
0 1 10 50 nmol/l
LDLR
0 0.2 0.5 1 2 5 10 50 nmol/l
β-actin

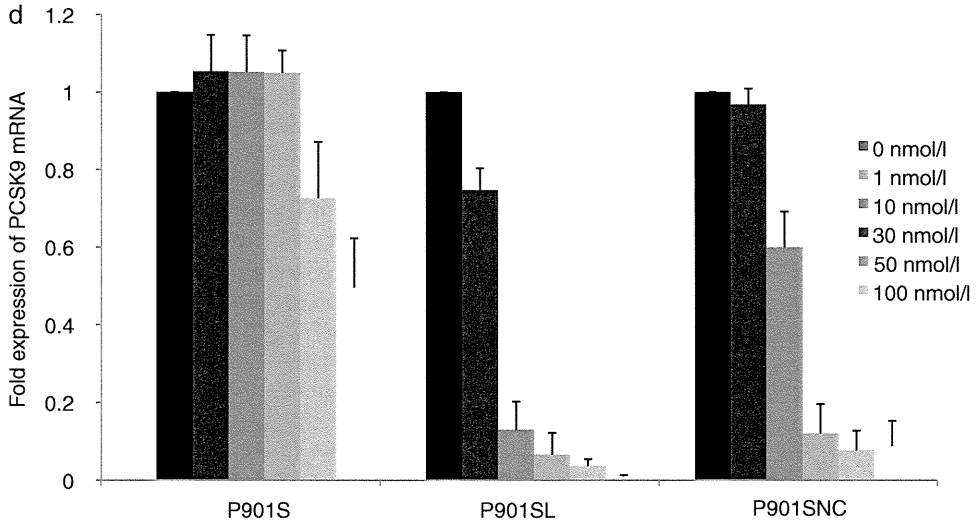
d
Fold expression of PCSK9 mRNA
1.2
1
0.8
0.6
0.4
0.2
0
P901S
P901SL
P901SNC
0 nmol/l
1 nmol/l
10 nmol/l
30 nmol/l
50 nmol/l
100 nmol/l

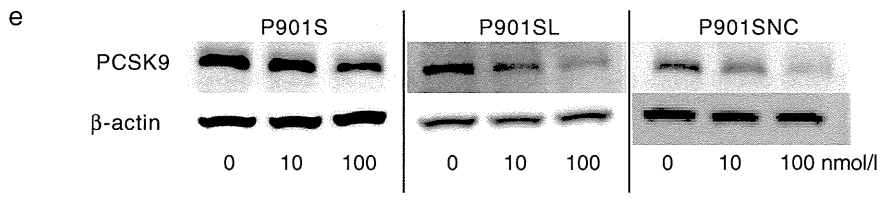
e
P901S
P901SL
P901SNC
PCSK9
β-actin
0 10 100
0 10 100
0 10 100 nmol/l

the cholesterol content of each lipoprotein fraction was measured. P901SL showed no significant reduction of LDL-C levels, whereas P901SNC reduced serum LDL-C levels by ~30% at the highest dose (10 mg/kg/injection), and the reduction occurred in a dose-dependent manner (**Figure 7a**). We observed a slower onset of the reduction of LDL-C of P901SL 6 weeks after the first treatment (**Supplementary Figure S2**). Meanwhile, hepatic PCSK9 mRNA expression was suppressed and the hepatic LDLR protein was increased accompanied by AON treatment with relatively large deviations (**Figure 7b,c**). PCSK9 mRNA was inhibited by P901SL and P901SNC as efficiently as P900SL. LDLR protein responded maximally to 20 mg/kg/injection of P901SL and 10 mg/kg/injection of P901SNC. The increasing rates of these two arms were nearly the same (~1.5-fold increase). The lack of severe hepatotoxicities or kidney toxicities was confirmed by serum chemistry in both the P901SL- and P901SNC-treated arms (**Supplementary Table S3**). Collectively, 2′,4′-BNA^{NC}–based AON, P901SNC, was as safe as the 2′,4′-BNA–based counterpart, P901SL.

Discussion

We demonstrated in this article that BNA-based antisense therapeutics successfully inhibited hepatic PCSK9 expression, resulting in a strong reduction of the serum LDL-C levels of mice. Our findings support the hypothesis that PCSK9 is a potential therapeutic target for hypercholesterolemia. To the best of our knowledge, this is the first time that we were able to show that BNA-based AONs induced cholesterol-lowering action in hypercholesterolemic mice. P900SL yielded high inhibitory activity *in vivo* as well as *in vitro*, and i.v. administration gave the highest peak inhibitory activity of the three representative routes. Nevertheless, i.p. and s.c. injections are alternative routes to i.v. injection, because they yielded adequate dose-responsive suppression of PCSK9 mRNA. In fact, Mipomersen for the treatment of hypercholesterolemia is given s.c. rather than i.p. due to practicality.[33,34] The rationality of s.c. injection is also supported by the pharmacokinetic nature and disposition properties of 2′-*O*-methyl phosphorothioate AON.[35] The peak tissue levels of 2'-*O*-methyl phosphorothioate AON after i.v. injection were higher than after s.c. and i.p. administration, and i.v. injection gives the peak of exon skipping efficiency. However, the bioavailability of 2′-*O*-methyl phosphorothioate AON was similar among all routes, and durable effects were observed after s.c. administration; therefore, the investigators selected s.c. administration for a preclinical study in mice. On the other hand, the hepatic accumulation of P900SL associated with a single i.v. injection increased directly with dose. This result was totally consistent with a 2′,4′-BNA gapmer targeting apolipoprotein B.[29] Further research to elucidate the pharmacokinetics of BNA-AONs is now underway.

The *in vivo* silencing properties of 2′,4′-BNA–based AON that targets PCSK9 mRNA were previously reported by Gupta *et al.*[20] They achieved the silencing of PCSK9 concomitantly with the upregulation of hepatic LDLR in female mice. However, they did not mention the cholesterol-lowering effect of the 2′,4′-BNA–based AON. We observed a dose-dependent decrease of LDL-C levels and a dose-dependent increase of HDL-C levels (**Figure 5**). There seems to be no trend in the net changes of serum total cholesterol levels (**Supplementary Table S1**). The increase in LDLR protein levels reported by Gupta *et al.*[20] were a little higher than those in **Figure 5d**. The likely explanation is the difference of experimental conditions in which they have used female NMRI mice with standard maintenance diet, whereas we used male C57BL/6J mice with atherogenic diet which contains 1.25% of cholesterol, 0.5% of cholic acid, and so on. Hepatic influx of these ingredients in the diet are known to strongly induce the downregulation of LDLR and cholesterol biosynthetic enzymes such as HMG-CoA reductase by downregulating SREBPs, important transcriptional factors, which results in LDLR reduction.[13,36,37] We also observed dose-dependent moderate increases of aspartate aminotransferase, ALT, and blood urea nitrogen levels, whereas histopathological analysis revealed no severe hepatic toxicities (**Figure 6**, **Supplementary Table S2**). Collectively, a continuous dosing of P900SL showed potent LDL-C reduction in mice without severe side effects, and this report provides the experimental proof of the cholesterol-lowering effects of BNA-based AONs.

We also achieved a dose-dependent decrease in serum LDL-C levels by using a 2′,4′-BNA^{NC}–based AON (P901SNC) (**Figure 7a**). In this case, serum HDL-C levels and the levels of liver and kidney toxicity indicators were not elevated (**Supplementary Table S3**). When compared with P901SNC, a delayed decrease of LDL-C levels was observed in the P901SL-treated arm (**Supplementary Figure S2**). We also showed here that a 2′,4′-BNA^{NC}–based AON (P901SNC) has greater potential to inhibit PCSK9 and to reduce serum cholesterol levels with no toxicity than a conventional 2′,4′-BNA–based AON. The high-potency and low-toxicity characteristics of a 2′,4′-BNA^{NC}–based AON were previously reported to effectively inhibit PTEN mRNA without elevation of the serum ALT level, whereas elevated serum ALT was observed in the 2′,4′-BNA counterpart-treated arm.[26] Thus, we conclude that 2′,4′-BNA^{NC}–based AONs can be a promising therapeutic agent for antisense therapy. However, the structure-activity relationship of BNA-based AONs still remains to be elucidated.

As previously reported, LDLR mRNA expression was independent of PCSK9 inhibition.[20,27] The coordinate repression of SREBP2, HMG-CoA synthase, and ABCA1 is in agreement with a response to a transient massive influx of cholesterol in the liver (**Figure 5e**). HMG-CoA synthase and ABCA1 are both known to be regulated by SREBP2, whereas SR-B1 and ACAT1 are atypical factors regulated by SREBP2.[3,4] The mRNA expression levels of the latter two factors were unchanged by P900SL, while an increased expression level of CYP7A1 was induced by P900SL. CYP7A1 is the first and

Figure 2 *In vitro* silencing properties of AONs (CR01S, CR01SL, P900S, P900SL, P901SL, and P901SNC). AONs were transfected into NMuLi cells. (**a,b**) After a 24-hour incubation, cells were collected and the expression levels of PCSK9 mRNA were determined. Data represent means ± SD. (**c**) PCSK9 and LDLR proteins were also detected by western blotting. AONs (P901S, P901SL, and P901SNC) were transfected into HepG2 cells. (**d**) After a 24-hour incubation, HepG2 cells were collected and the expression levels of PCSK9 mRNA were determined. Data represent mean values ± SD. (e) PCSK9 and β-actin proteins were detected by western blotting. AON, antisense oligonucleotide; LDLR, low-density lipoprotein receptor; mRNA, messenger RNA.

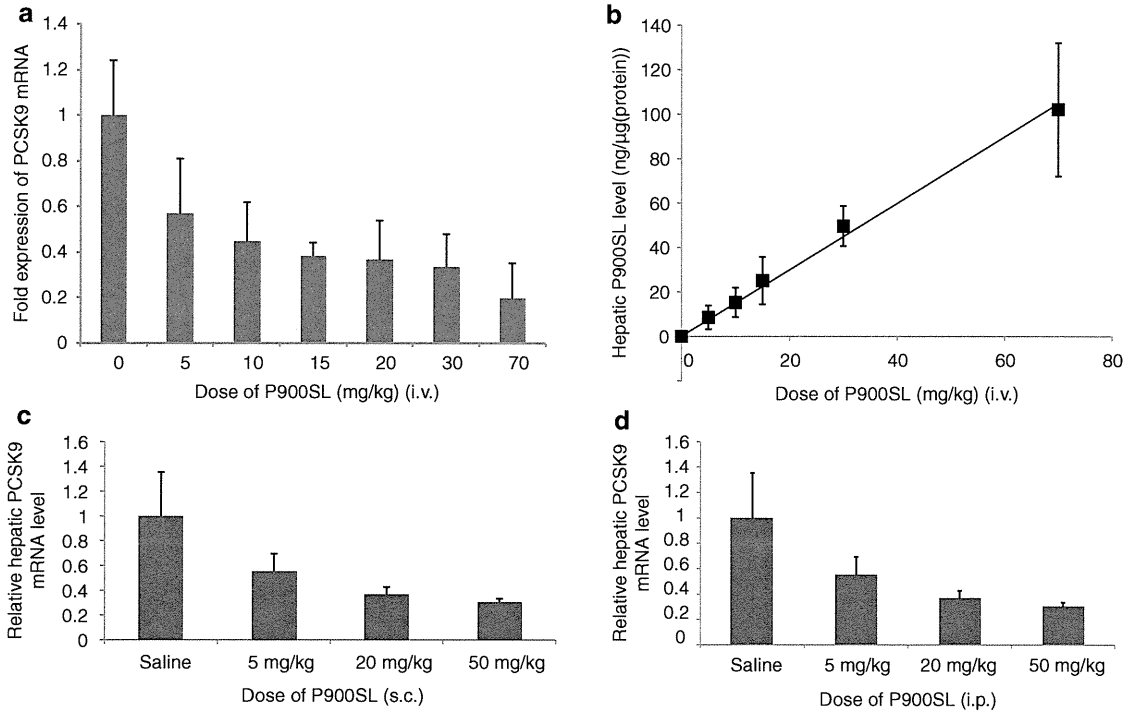

Figure 3 Single administration of P900SL to normal-chow fed C57BL/6J mice. (**a**,**b**) Hepatic PCSK9 messenger RNA (mRNA) level and P900SL content 72 hours after a single intravenous (i.v.) administration were expressed as a function of dose level. (**c**,**d**) Liver PCSK9 mRNA expression level was measured and presented for each dose 72 hours after subcutaneous (s.c.) and intraperitoneal (i.p.) injection, respectively. Data represent mean values ± SD. $n = 4–7$.

rate-limiting enzyme in bile acid synthesis; bile acids are versatile signaling molecules that play critical roles in maintaining the homeostasis of cholesterol, lipid, glucose, and energy.[38,39] CYP7A1 deficiency in humans is associated with dyslipidemia, the formation of gallstones, and atherosclerosis.[40] A previous report showed that C57BL/6J mice overexpressing CYP7A1 are less susceptible to atherogenic diet-induced elevations of very low-density lipoprotein, intermediate-density lipoprotein, and LDL-C and to reductions of HDL-C and triglyceride and less susceptible to the formation of gallstones and atherosclerosis than their nontransgenic littermates.[41,42] Similarly, under atherogenic conditions, we observed a reduction in the serum LDL-C level and induction of HDL-C in P900SL-treated mice; these effects may be partly due to the induction of CYP7A1 to maintain intrahepatic cholesterol homeostasis. Collectively, we observed the strong induction of CYP7A1 mRNA associated with the strong suppression of PCSK9. Further investigation of underlying mechanisms of PCSK9 inhibition in atherogenic diet-fed mice are necessary to extrapolate the cholesterol-lowering efficacy of PCSK9 inhibitors in humans.

In conclusion, we found that the strong inhibition of PCSK9 by BNA-based AONs can greatly reduce serum LDL-C levels in atherogenic diet-fed mice *via* a novel mechanism of CYP7A1 upregulation. These results indicate that PCSK9 is an excellent drug target for the treatment of hypercholesterolemia. Although a structure of AON has not been fully optimized yet here, the 2′,4′-BNA^{NC}–based AON shows higher potency than its 2′,4′-BNA counterpart and like 2′,4′-BNA shows no toxicity under the conditions tested. Meanwhile, a recent report from Gupta *et al.* demonstrated the superiority of a shorter AON with a smaller number of 2′,4′-BNA modifications over a conventional 20-mer 2′,4′-BNA-gapmer in an antisense potency. They have used a 13-mer AON with five 2′,4′-BNAs and eight gaps that efficiently inhibit the expression of PCSK9 mRNA and protein. We suppose that 2′,4′-BNA^{NC}–based AON also has its own unique optimal structure and a further optimization of sequence, length, and composition of 2′,4′-BNA^{NC}–based AONs would provide a more reliable 2′,4′-BNA^{NC}–based PCSK9 inhibitor.

Materials And Methods

AONs. Two types of modified nucleic acids, 2′,4′-BNA and 2′,4′-BNA^{NC}, were partially incorporated into 20-mer phosphorothioated oligodeoxyribonucleotides with various sequences. CR01S and CR01SL were 20-mer phosphorothioate DNA and 2′,4′-BNA–modified AON, respectively, designed not to target any gene in mice. P900S and P900SL were designed to target murine PCSK9 mRNA, and their sequences have been reported previously. P901S, P901SL, and P901SNC target an identical consensus sequence on mice and human PCSK9 mRNA but have different chemistries. The exact sequences of molecules used in this study are presented in **Table 1**. A large-scale synthesis of 2′,4′-BNA^{NC} units was conducted by BNA (Osaka, Japan). All 2′,4′-BNA^{NC} monomer units were obtained from BNA. All modified oligonucleotides were provided by Gene Design (http://www.genedesign.co.jp/). The syntheses were conducted by standard phosphoramidite procedures, and products were carefully processed under aseptic conditions and purified. All

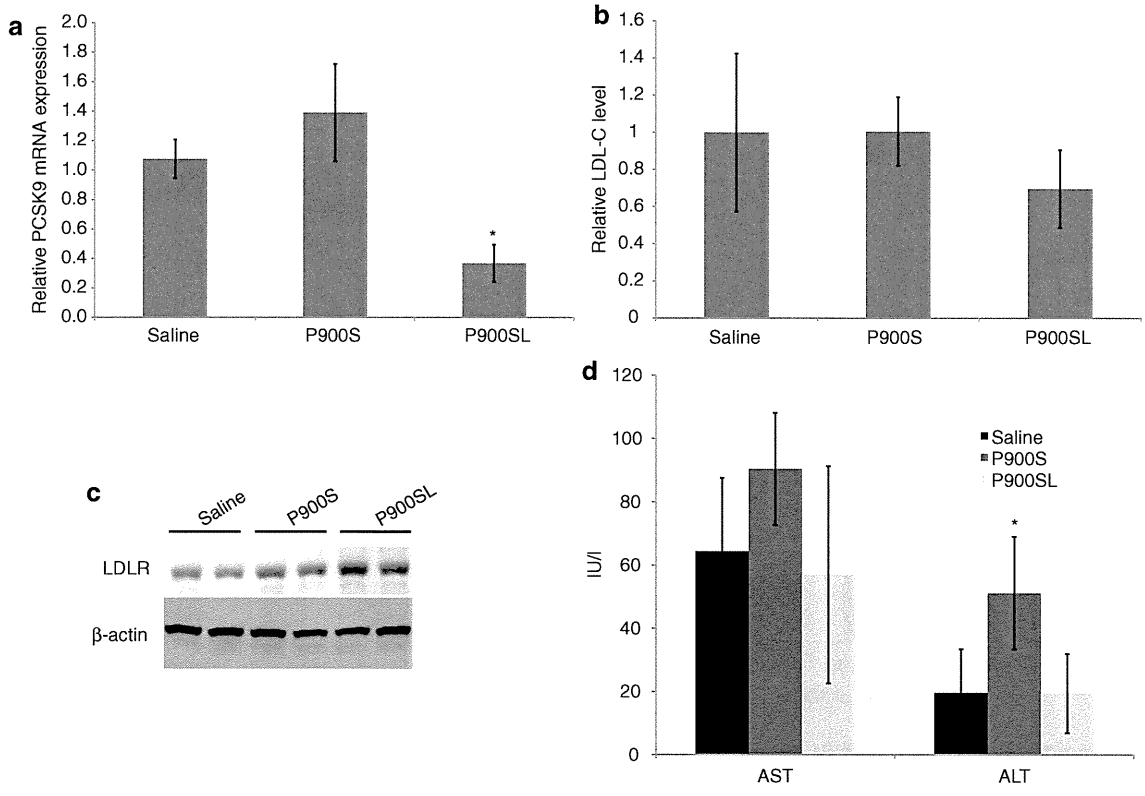

Figure 4 Short-term effects of P900S and P900SL. Atherogenic diet-fed mice received intraperitoneal administration of P900S or P900SL at a dose of 10 mg/kg twice during 4 days. (**a**) Liver PCSK9 mRNA levels 4 days after the first injection. (**b**) Relative serum LDL-C levels 4 days after the first injection. (**c**) Hepatic LDLR protein expression levels were estimated by western blotting. (**d**) Serum liver transaminases (AST, ALT) were analyzed. Data represent mean values (± SD). *$P < 0.05$. ALT, alanine aminotransferase; AST, aspartate aminotransferase; LDL-C, low-density lipoprotein cholesterol; LDLR, low-density lipoprotein receptor; mRNA, messenger RNA.

products were endotoxin-free and contained low levels of residual salts for *in vivo* usage.

In vitro transfection procedures. For AON transfection experiments, NMuLi cells or HepG2 cells were seeded at 5.0×10^5 cells per well in 6-well plates. AONs were transfected by using Lipofectamine 2000 (Invitrogen, Carlsbad, CA) according to the manufacturer's procedures. After a 4-hour transfection, cells were continuously incubated for an additional 20 hours at 37 °C. After incubation, cells were collected and subjected to subsequent analyses.

In vivo pharmacological experiments. All animal procedures were performed in accordance with the guidelines of the Animal Care Ethics Committee of the National Cerebral and Cardiovascular Center Research Institute (Osaka, Japan). All animal studies were approved by an institutional review board. C57BL/6J mice were obtained from CLEA Japan (Tokyo, Japan). All mice were male, and studies were initiated when animals were 6–8 weeks of age. Mice were maintained on a 12-hour light/dark cycle and fed *ad libitum*. Mice were fed a normal chow (CE-2; CLEA Japan) or an artery-hardening food, F2HFD1 (Oriental Yeast, Tokyo, Japan) for 2 weeks before the first treatment and during treatment. Mice received single or multiple treatments of AONs administered i.v, i.p. or s.c. in the dose range of 1–70 mg/kg/injection. Peripheral blood was collected from a tail vein in BD Microtainers (BD, Franklin Lakes, NJ) for separation of serum. Lipid component analysis of serum was performed by Skylight Biotech (http://www.skylight-biotech.com/). At the time of sacrifice, mice were anesthetized with diethyl ether (Wako, Osaka, Japan). Livers were harvested and snap-frozen until subsequent analysis. Whole blood was collected and subjected to serum separation for subsequent analysis.

mRNA quantification. Total RNA was isolated from cultured cells or mouse liver tissues by using TRIzol Reagent (Invitrogen) according to the manufacturer's procedure. Gene expression was evaluated by a two-step quantitative reverse transcription-PCR method. Reverse-transcription of RNA samples was performed by using a High Capacity cDNA Reverse-Transcription Kit (Applied Biosystems, Foster City, CA), and quantitative PCR was performed by a Fast SYBR Green System or TaqMan Gene Expression Assays (Applied Biosystems). The mRNA levels of target genes were normalized to the GAPDH mRNA level. The following primer sets were used for quantitative PCRs. Ror murine PCSK9; forward: 5′-TCAGTTCTGCACACCTCCAG-3′, reverse: 5′-GGG TAAGGTGCGGTAAGTCC-3′ and forward: 5′-GCTCAACTG TCAAGGGAAGG-3′, reverse: 5′-CGTTGAGGATGCGGCTA TAC-3′. For human PCSK9; forward: 5′-AAGGGAAGGG CACGGTTAG-3′, reverse: 5′-GAGTAGAGGCAGGCATCG TC-3′. For murine GAPDH; forward: 5′-GTGTGAACGGATTT GGCCGT-3′, reverse: 5′-GACAAGCTTCCCATTCTCGG-3′

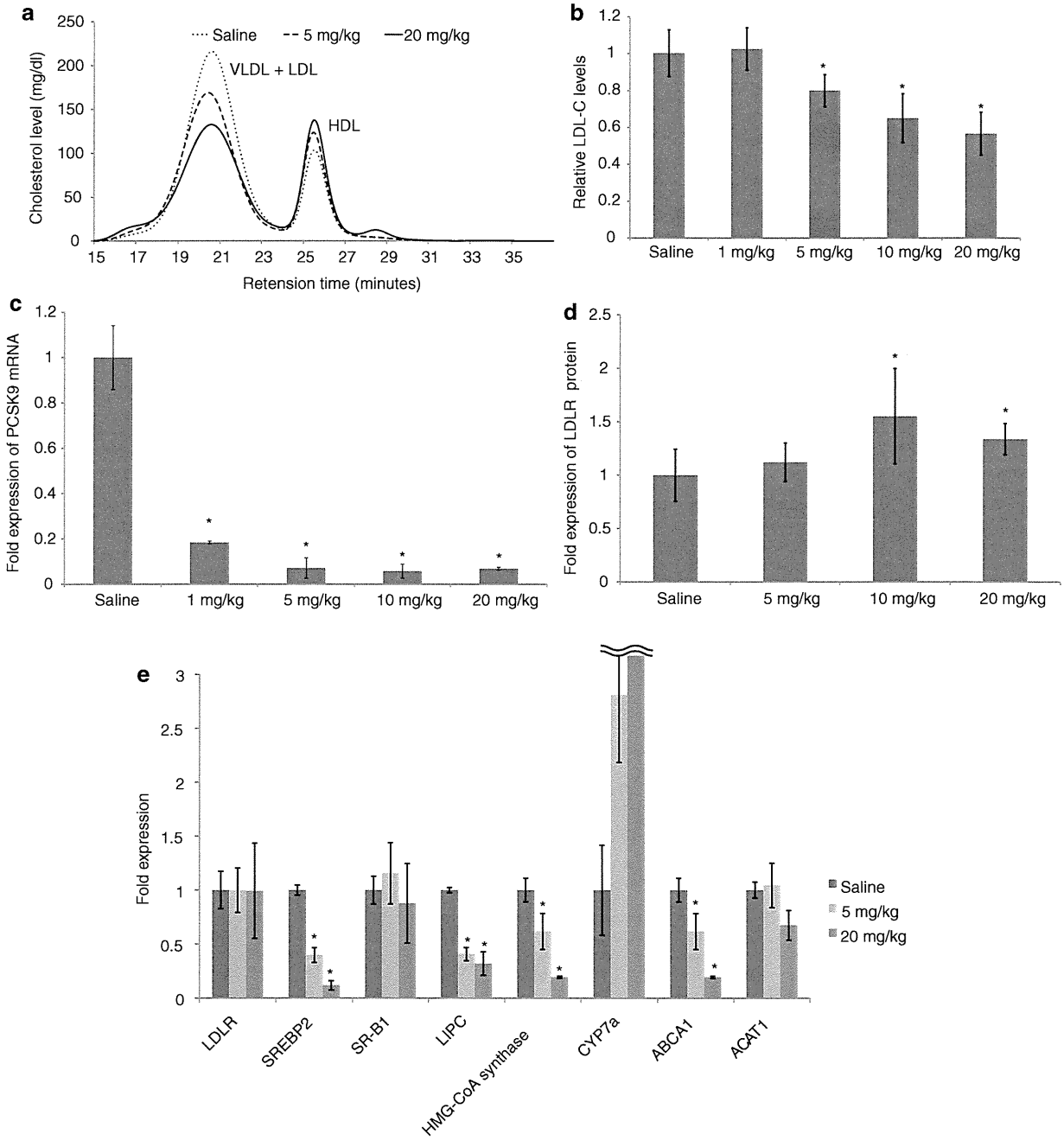

Figure 5 Dose-dependent responses of physiological parameters to P900SL dosing. (**a**) Changes in cholesterol fractions upon administration of P900SL analyzed by HPLC. (**b**) Ratio of serum LDL-C levels after 4 weeks of treatment to before treatment were arranged in order of doses. (**c**) Liver PCSK9 mRNA levels were measured at all dose levels after 6 weeks of treatment. (**d**) Hepatic LDLR protein levels were determined 6 weeks after treatment started. (**e**) The expression levels of genes regulating lipid homeostasis in liver were analyzed. Data represent mean values ± SD. $^*P < 0.05$. $n = 5$. HDL, high-density lipoprotein; HPLC, high performance liquid chromatography; LDL, low-density lipoprotein; LDL-C, LDL cholesterol; LDLR, LDL receptor; mRNA, messenger RNA; VLDL, very LDL.

and for human GAPDH; forward: 5′-GAGTCAACGG ATTTGGTCGT-3′, reverse: 5′-GACAAGCTTCCCGTTCTC AG-3′. For murine LDLR, SREBP2, SR-BI, LIPC, HMGCS2, CYP7A1, ABCA1, and ACAT1, TaqMan Gene Expression Assays were used; assay IDs: Mm00440169_ m1,Mm01306297_g1,Mm00450236_m1,Mm01147313_m1, Mm00550050_m1, Mm00484152_m1, Mm01350760_m1, Mm00507463_m1, respectively.

Western blotting analysis. Cultured cells and frozen liver tissues were suspended in lysis buffer (150 mmol/l NaCl, 1.0% IGEPAL CA-630, 0.5% sodium deoxycholate, 0.1% SDS, 50 mmol/l Tris, pH 8.0, 20 × Complete Mini protease inhibitor cocktail 1:20 (Roche, Indianapolis, IN)) and homogenized with TissueLyser II (Qiagen, Valencia, CA). Total protein concentrations were measured with a detergent compatible assay kit (Bio-Rad, Hercules, CA). Solutions were subjected

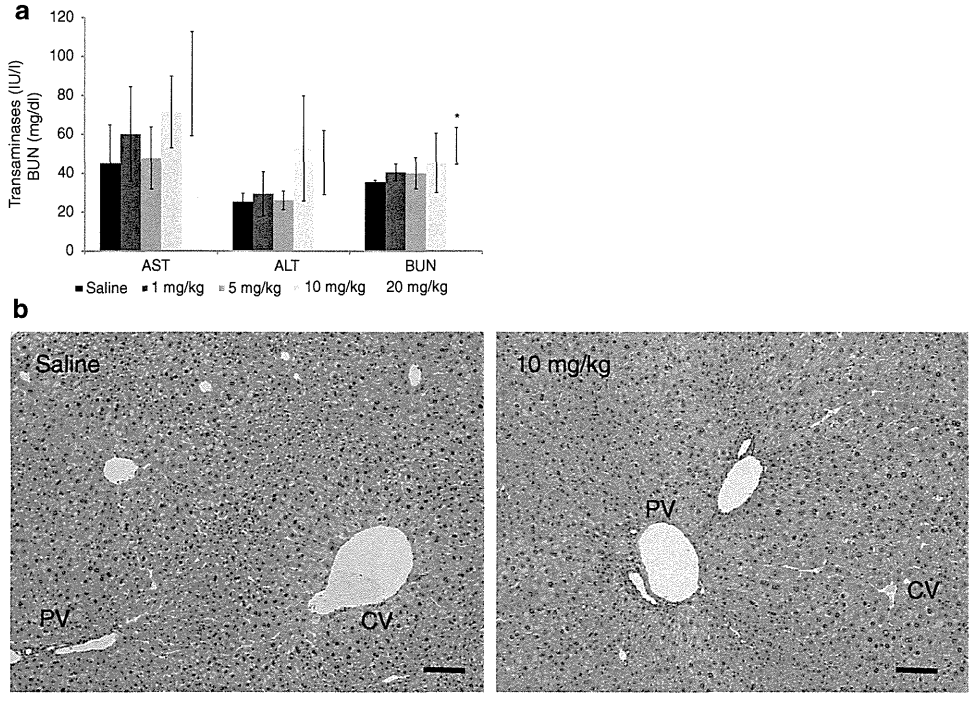

Figure 6 Changes in toxicological parameters upon P900SL dosing. (a) Serum liver transaminases (AST and ALT) and BUN levels were measured. Data represent mean values ± SD. $^*P < 0.05$. **(b)** Representative H&E stain images of liver of saline- and P900SL-treated mice. Bar indicates 100 μm. AST, aspartate aminotransferase; ALT, alanine aminotransferase; BUN, blood urea nitrogen; CV, central vein; H&E, hematoxylin and eosin; PV, portal vein.

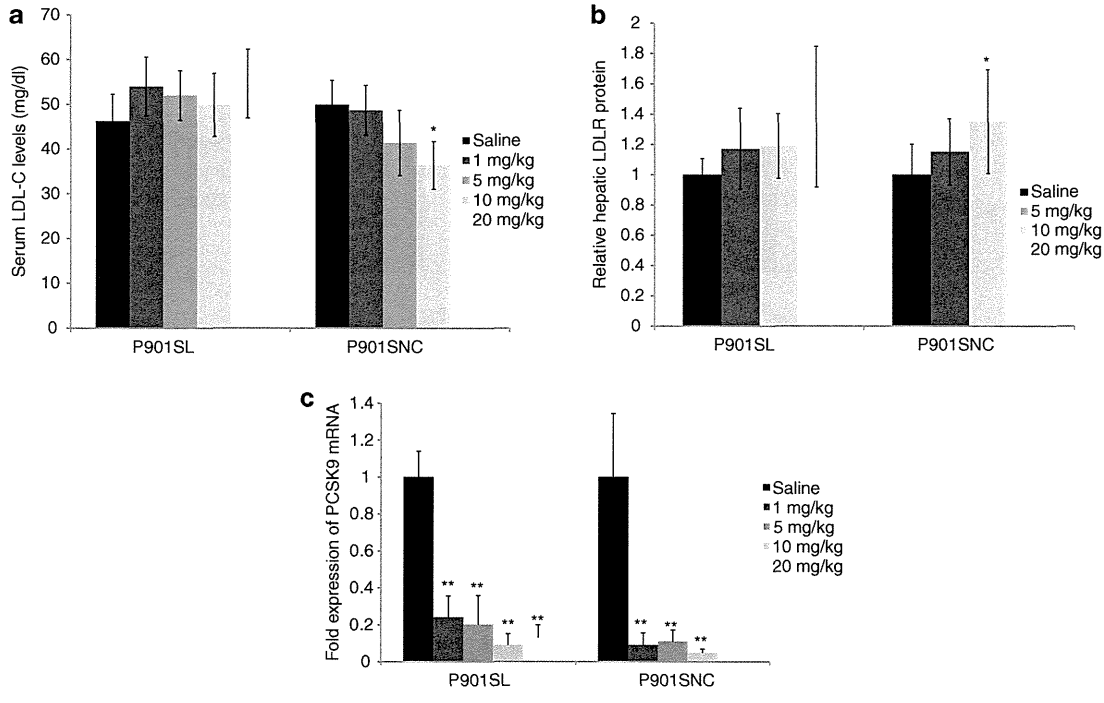

Figure 7 Dose-dependent and chemistry-dependent differences in serum LDL-C levels, hepatic LDLR protein, and PCSK9 mRNA levels after treatment of P901SL and P901SL. (a) Raw values of serum LDL-C were obtained at 4th week of schedule. **(b)** Hepatic LDLR protein expression levels were measured after the end of the schedule. **(c)** Liver PCSK9 mRNA levels were measured at all dose levels after 6 weeks of treatment. Data represent mean values ± SD. $^*P < 0.05$, $^{**}P < 0.001$ (versus a saline-treated control arm). $n = 5$. LDL-C, low-density lipoprotein cholesterol; LDLR, low-density lipoprotein receptor; mRNA, messenger RNA.

to electrophoresis on 16 or 6% Tris-glycine gels (Invitrogen) and transferred to a polyvinylidene difluoride membrane (Bio-Rad). PCSK9 western blotting was performed at room temperature for 1 hour with a primary anti-rabbit PCSK9 antibody (1:200; Abcam, Cambridge, UK). Additional analyses were performed by using anti-LDLR antibody (R&D Systems, Minneapolis, MN) and anti-β actin antibody (Cell Signaling Technology, Danvers, MA). Membranes were washed three times with phosphate-buffered saline containing 0.3% Tween 20. Blots were labeled by using horseradish peroxidase-conjugated secondary antibodies, either goat anti-rabbit or donkey anti-goat antibodies (Santa Cruz Biotechnology, Santa Cruz, CA). Chemiluminescent detection was performed by using an ECL plus Western blot detection kit (Amersham Biosciences, Buckinghamshire, UK), and bands were visualized by using an LAS-4000mini image analyzer (Fuji Film, Tokyo, Japan). β-Actin expression levels were used as an internal standard.

The determination of P900SL content in liver

Materials and reagents. The template DNA was a 29-mer DNA (5′-gaatagcgaggataatgtgctatgagccc-3′), which is complementary to P900SL, with biotin at the 3′-end. The ligation probe DNA was a 9-mer DNA (5′-tcgctattc-3′) with phosphate at the 5′-end and digoxigenin at the 3′-end. The template DNA and the ligation probe DNA were purchased from Japan Bio Services (Saitama, Japan). Reacti-Bind NeutrAvidin-coated polystyrene strip plates were purchased from Thermo Fisher Scientific (Waltham, MA) (nunc immobilizer streptavdin F96 white, 436015). The template DNA solution (100 nmol/l) was prepared in hybridization buffer containing 60 mmol/l Na_2HPO_4 (pH 7.4), 0.9 mol/l NaCl, and 0.24% Tween 20. The ligation probe DNA solution (200 nmol/l) was prepared in 1.5 units/well of T4 DNA ligase (TaKaRa, Shiga, Japan) with 66 mmol/l Tris-HCl (pH 7.6), 6.6 mmol/l $MgCl_2$, 10 mmol/l DTT, and 0.1 mmol/l ATP.

The washing buffer used throughout the assay contained 25 mmol/l Tris-HCl (pH 7.2), 0.15 mol/l NaCl, and 0.1% Tween 20. Anti-digoxigenin-AP antibody (Fab fragments conjugated with alkaline phosphatase) was obtained from Roche Diagnostics. A 1:2,000 dilution of the antibody with 1:10 super block buffer in TBS (Pierce, Rockford, IL) was used in the assay. The alkaline phosphatase luminous substrate was prepared in 250 μmol/l CDP-Star (Roche) with 100 mmol/l Tris-HCl (pH 7.6) and 100 mmol/l NaCl.

Sample preparation. Frozen liver tissue was collected in a 2-ml tube with 1 ml of phosphate-buffered saline and a zirconia ball (ø 5 mm; Irie, Tokyo, Japan) and mechanically homogenized for 2 minutes at 30 oscillations per second by a TissueLyser II apparatus (Qiagen). Total protein concentrations were measured with a detergent compatible assay kit (Bio-Rad) and adjusted to 8 mg/l with phosphate-buffered saline. The assay was performed at the concentration range of 128 pmol/l–400 nmol/l in duplicate. For the standard curve, 10 standard solutions were prepared. To AON-untreated mice, liver homogenates were added to P900SL solutions to prepare 10 standard samples at a range of 128 pmol/l–400 nmol/l.

Assay procedures. The template DNA solution (100 μl) and standard solution (10 μl) or liver homogenates (10 μl) containing the P900SL were added to Reacti-Bind Neutr Avidin-coated polystyrene strip 96-well plates and incubated at 37 °C for 1 hour to allow the binding of biotin to streptavidin-coated wells and hybridization. After hybridization, the plate was washed three times with 200 μl of washing buffer. Then, ligation probe DNA solution (100 μl) was added, and the plate was incubated at room temperature (15 °C) for 3 hours. The plate was then washed three times with the washing buffer. Subsequently, 200 μl of a 1:2,000 dilution of anti-digoxigenin-AP was added, and the plate was incubated at 37 °C for 1 hour. After washing three times with the washing buffer, CDP-Star solution was added to the plate, and finally the luminescence intensity was determined by using a Centro XS^3 luminometer (Berthold Technologies, Bad Wildbad, Germany) one second after the addition of CDP-Star. The linear range of 128 pmol/l–400 nmol/l in this ELISA system was determined as $r > 0.99$.

Serum chemistry and hematoxylin and eosin staining. Serum from blood collected from the inferior vena cava upon sacrifice was subjected to serum chemistry. Assay kits (WAKO) were used to measure serum levels of aspartate aminotransferase, ALT, blood urea nitrogen, and creatinine, which are biomarkers for hepatic and kidney toxicities. Formalin-fixed liver samples (20% formalin; WAKO) were sliced by microtome (Leica Microsystems, Wetzlar, Germany), embedded in Histsec (Merck, Darmstadt, Germany) and stained with Carrazzi's hematoxylin and Tissue-Tek eosin solutions.

Statistical analysis. Pharmacological studies were performed with 5–7 mice per treatment group. A Student's *t*-test was performed for comparison of two arms. $P < 0.05$ or $P < 0.01$ was considered to be of statistical significance.

Supplementary Material

Figure S1. Comparison of intrahepatic cholesterol levels between control and 20 mg/kg/injection of P900SL-treated arms.

Figure S2. Relation between given dose and serum LDL-C levels of P901SL 6 weeks after treatment started.

Table S1. Serum raw cholesterol levels in atherogenic diet-fed mice after 4 weeks of P900SL treatment.

Table S2. Summary of histopathological findings.

Table S3. Toxicological parameters.

Materials and Methods.

Acknowledgments. We thank Eiko Shibata, Mai Inoue, Megumu Morimoto, and Manami Sone for their technical support, who are affiliated with National Cerebral and Cardiovascular Center Research Institute. A part of this work was supported by the Program for Promotion of Fundamental Studies in Health Sciences of the National Institute of Biomedical Innovation (NIBIO) and a research grant from the Ministry of Health, Labor, and Welfare (H23-seisakutansaku-ippan-004). T.Y. thanks the Research Fellowship from the Japan Society for the Promotion of Science (JSPS) for Young Scientists. T.I. is a CEO of BNA Inc., the company that produces 2′,4′-BNA^{NC} monomers. The other authors declared no conflict of interest.

1. Jones, P, Kafonek, S, Laurora, I and Hunninghake, D (1998). Comparative dose efficacy study of atorvastatin versus simvastatin, pravastatin, lovastatin, and fluvastatin in patients with hypercholesterolemia (the CURVES study). *Am J Cardiol* **81**: 582–587.

2. Goldstein, JL and Brown, MS (2009). The LDL receptor. *Arterioscler Thromb Vasc Biol* **29**: 431–438.
3. Horton, JD, Goldstein, JL and Brown, MS (2002). SREBPs: activators of the complete program of cholesterol and fatty acid synthesis in the liver. *J Clin Invest* **109**: 1125–1131.
4. Horton, JD, Shah, NA, Warrington, JA, Anderson, NN, Park, SW, Brown, MS *et al.* (2003). Combined analysis of oligonucleotide microarray data from transgenic and knockout mice identifies direct SREBP target genes. *Proc Natl Acad Sci USA* **100**: 12027–12032.
5. Kong, WJ, Liu, J and Jiang, JD (2006). Human low-density lipoprotein receptor gene and its regulation. *J Mol Med* **84**: 29–36.
6. Issandou, M (2006). Pharmacological regulation of low density lipoprotein receptor expression: current status and future developments. *Pharmacol Ther* **111**: 424–433.
7. Zelcer, N and Tontonoz, P (2006). Liver X receptors as integrators of metabolic and inflammatory signaling. *J Clin Invest* **116**: 607–614.
8. Garcia, CK, Wilund, K, Arca, M, Zuliani, G, Fellin, R, Maioli, M *et al.* (2001). Autosomal recessive hypercholesterolemia caused by mutations in a putative LDL receptor adaptor protein. *Science* **292**: 1394–1398.
9. Harada-Shiba, M, Takagi, A, Miyamoto, Y, Tsushima, M, Ikeda, Y, Yokoyama, S *et al.* (2003). Clinical features and genetic analysis of autosomal recessive hypercholesterolemia. *J Clin Endocrinol Metab* **88**: 2541–2547.
10. Abifadel, M, Varret, M, Rabès, JP, Allard, D, Ouguerram, K, Devillers, M *et al.* (2003). Mutations in PCSK9 cause autosomal dominant hypercholesterolemia. *Nat Genet* **34**: 154–156.
11. Zelcer, N, Hong, C, Boyadjian, R and Tontonoz, P (2009). LXR regulates cholesterol uptake through Idol-dependent ubiquitination of the LDL receptor. *Science* **325**: 100–104.
12. Lambert, G, Charlton, F, Rye, KA and Piper, DE (2009). Molecular basis of PCSK9 function. *Atherosclerosis* **203**: 1–7.
13. Maxwell, KN, Soccio, RE, Duncan, EM, Sehayek, E and Breslow, JL (2003). Novel putative SREBP and LXR target genes identified by microarray analysis in liver of cholesterol-fed mice. *J Lipid Res* **44**: 2109–2119.
14. Attie, AD and Seidah, NG (2005). Dual regulation of the LDL receptor–some clarity and new questions. *Cell Metab* **1**: 290–292.
15. Cameron, J, Ranheim, T, Kulseth, MA, Leren, TP and Berge, KE (2008). Berberine decreases PCSK9 expression in HepG2 cells. *Atherosclerosis* **201**: 266–273.
16. Kong, W, Wei, J, Abidi, P, Lin, M, Inaba, S, Li, C *et al.* (2004). Berberine is a novel cholesterol-lowering drug working through a unique mechanism distinct from statins. *Nat Med* **10**: 1344–1351.
17. Kong, WJ, Wei, J, Zuo, ZY, Wang, YM, Song, DQ, You, XF *et al.* (2008). Combination of simvastatin with berberine improves the lipid-lowering efficacy. *Metab Clin Exp* **57**: 1029–1037.
18. Chan, JC, Piper, DE, Cao, Q, Liu, D, King, C, Wang, W *et al.* (2009). A proprotein convertase subtilisin/kexin type 9 neutralizing antibody reduces serum cholesterol in mice and nonhuman primates. *Proc Natl Acad Sci USA* **106**: 9820–9825.
19. Frank-Kamenetsky, M, Grefhorst, A, Anderson, NN, Racie, TS, Bramlage, B, Akinc, A *et al.* (2008). Therapeutic RNAi targeting PCSK9 acutely lowers plasma cholesterol in rodents and LDL cholesterol in nonhuman primates. *Proc Natl Acad Sci USA* **105**: 11915–11920.
20. Gupta, N, Fisker, N, Asselin, MC, Lindholm, M, Rosenbohm, C, Ørum, H *et al.* (2010). A locked nucleic acid antisense oligonucleotide (LNA) silences PCSK9 and enhances LDLR expression *in vitro* and in vivo. *PLoS ONE* **5**: e10682.
21. Swayze, EE, Siwkowski, AM, Wancewicz, EV, Migawa, MT, Wyrzykiewicz, TK, Hung, G *et al.* (2007). Antisense oligonucleotides containing locked nucleic acid improve potency but cause significant hepatotoxicity in animals. *Nucleic Acids Res* **35**: 687–700.
22. Yamamoto, T, Nakatani, M, Narukawa, K and Obika, S (2011). Antisense drug discovery and development. *Future Med Chem* **3**: 339–365.
23. Rahman, SM, Seki, S, Obika, S, Yoshikawa, H, Miyashita, K and Imanishi, T (2008). Design, synthesis, and properties of 2',4'-BNA(NC): a bridged nucleic acid analogue. *J Am Chem Soc* **130**: 4886–4896.
24. Obika, S, Rahman, SMA, Fujisaka, A, Kawada, Y, Baba, T and Imanishi, T (2010). Bridged nucleic acids: development, synthesis, and properties. *Heterocycles* **81**: 1347–1392.
25. Miyashita, K, Rahman, SMA, Seki, S, Obika, S and Imanishi, T (2007). N-Methyl substituted 2′,4′-BNA(NC): a highly nuclease-resistant nucleic acid analogue with high-affinity RNA selective hybridization. *Chem Commun*: 3765–3767.
26. Prakash, TP, Siwkowski, A, Allerson, CR, Migawa, MT, Lee, S, Gaus, HJ *et al.* (2010). Antisense oligonucleotides containing conformationally constrained 2',4'-(N-methoxy) aminomethylene and 2',4'-aminooxymethylene and 2'-O,4'-C-aminomethylene bridged nucleoside analogues show improved potency in animal models. *J Med Chem* **53**: 1636–1650.
27. Graham, MJ, Lemonidis, KM, Whipple, CP, Subramaniam, A, Monia, BP, Crooke, ST *et al.* (2007). Antisense inhibition of proprotein convertase subtilisin/kexin type 9 reduces serum LDL in hyperlipidemic mice. *J Lipid Res* **48**: 763–767.
28. Yu, RZ, Baker, B, Chappell, A, Geary, RS, Cheung, E and Levin, AA (2002). Development of an ultrasensitive noncompetitive hybridization-ligation enzyme-linked immunosorbent assay for the determination of phosphorothioate oligodeoxynucleotide in plasma. *Anal Biochem* **304**: 19–25.
29. Straarup, EM, Fisker, N, Hedtjärn, M, Lindholm, MW, Rosenbohm, C, Aarup, V *et al.* (2010). Short locked nucleic acid antisense oligonucleotides potently reduce apolipoprotein B mRNA and serum cholesterol in mice and non-human primates. *Nucleic Acids Res* **38**: 7100–7111.
30. Agrawal, S, Temsamani, J and Tang, JY (1991). Pharmacokinetics, biodistribution, and stability of oligodeoxynucleotide phosphorothioates in mice. *Proc Natl Acad Sci USA* **88**: 7595–7599.
31. Phillips, JA, Craig, SJ, Bayley, D, Christian, RA, Geary, R and Nicklin, PL (1997). Pharmacokinetics, metabolism, and elimination of a 20-mer phosphorothioate oligodeoxynucleotide (CGP 69846A) after intravenous and subcutaneous administration. *Biochem Pharmacol* **54**: 657–668.
32. Lendvai, G, Velikyan, I, Bergström, M, Estrada, S, Laryea, D, Välilä, M *et al.* (2005). Biodistribution of 68Ga-labelled phosphodiester, phosphorothioate, and 2'-O-methyl phosphodiester oligonucleotides in normal rats. *Eur J Pharm Sci* **26**: 26–38.
33. Akdim, F, Visser, ME, Tribble, DL, Baker, BF, Stroes, ES, Yu, R *et al.* (2010). Effect of mipomersen, an apolipoprotein B synthesis inhibitor, on low-density lipoprotein cholesterol in patients with familial hypercholesterolemia. *Am J Cardiol* **105**: 1413–1419.
34. Akdim, F, Stroes, ES, Sijbrands, EJ, Tribble, DL, Trip, MD, Jukema, JW *et al.* (2010). Efficacy and safety of mipomersen, an antisense inhibitor of apolipoprotein B, in hypercholesterolemic subjects receiving stable statin therapy. *J Am Coll Cardiol* **55**: 1611–1618.
35. Heemskerk, H, de Winter, C, van Kuik, P, Heuvelmans, N, Sabatelli, P, Rimessi, P *et al.* (2010). Preclinical PK and PD studies on 2'-O-methyl-phosphorothioate RNA antisense oligonucleotides in the mdx mouse model. *Mol Ther* **18**: 1210–1217.
36. Rudling, M (1992). Hepatic mRNA levels for the LDL receptor and HMG-CoA reductase show coordinate regulation in vivo. *J Lipid Res* **33**: 493–501.
37. Dueland, S, Drisko, J, Graf, L, Machleder, D, Lusis, AJ and Davis, RA (1993). Effect of dietary cholesterol and taurocholate on cholesterol 7 alpha-hydroxylase and hepatic LDL receptors in inbred mice. *J Lipid Res* **34**: 923–931.
38. Thomas, C, Pellicciari, R, Pruzanski, M, Auwerx, J and Schoonjans, K (2008). Targeting bile-acid signalling for metabolic diseases. *Nat Rev Drug Discov* **7**: 678–693.
39. Chiang, JY (2009). Bile acids: regulation of synthesis. *J Lipid Res* **50**: 1955–1966.
40. Pullinger, CR, Eng, C, Salen, G, Shefer, S, Batta, AK, Erickson, SK *et al.* (2002). Human cholesterol 7alpha-hydroxylase (CYP7A1) deficiency has a hypercholesterolemic phenotype. *J Clin Invest* **110**: 109–117.
41. Machleder, D, Ivandic, B, Welch, C, Castellani, L, Reue, K and Lusis, AJ (1997). Complex genetic control of HDL levels in mice in response to an atherogenic diet. Coordinate regulation of HDL levels and bile acid metabolism. *J Clin Invest* **99**: 1406–1419.
42. Miyake, JH, Duong-Polk, XT, Taylor, JM, Du, EZ, Castellani, LW, Lusis, AJ *et al.* (2002). Transgenic expression of cholesterol-7-alpha-hydroxylase prevents atherosclerosis in C57BL/6J mice. *Arterioscler Thromb Vasc Biol* **22**: 121–126.

Supplementary Information accompanies this paper on the Molecular Therapy–Nucleic Acids website (http://www.nature.com/mtna)

Biochimie 94 (2012) 1032–1040

Contents lists available at SciVerse ScienceDirect

Biochimie

journal homepage: www.elsevier.com/locate/biochi

Research paper

Chemical modification of triplex-forming oligonucleotide to promote pyrimidine motif triplex formation at physiological pH

Hidetaka Torigoe [a,*], Osamu Nakagawa [b], Takeshi Imanishi [b], Satoshi Obika [b], Kiyomi Sasaki [a]

[a] Department of Applied Chemistry, Faculty of Science, Tokyo University of Science, 1-3 Kagurazaka, Shinjuku-ku, Tokyo 162-8601, Japan
[b] Graduate School of Pharmaceutical Sciences, Osaka University, 1-6 Yamadaoka, Suita, Osaka 565-0871, Japan

ARTICLE INFO

Article history:
Received 21 June 2011
Accepted 4 January 2012
Available online 9 January 2012

Keywords:
Triplex formation
Chemical modification of triplex-forming oligonucleotide
Thermodynamic parameters
Rigidity
Hydration
Nuclease resistance

ABSTRACT

Extreme instability of pyrimidine motif triplex DNA at physiological pH severely limits its use in wide variety of potential applications, such as artificial regulation of gene expression, mapping of genomic DNA, and gene-targeted mutagenesis *in vivo*. Stabilization of pyrimidine motif triplex at physiological pH is, therefore, crucial for improving its potential in various triplex-formation-based strategies *in vivo*. To this end, we investigated the effect of 3′-amino-2′-*O*,4′-*C*-methylene bridged nucleic acid modification of triplex-forming oligonucleotide (TFO), in which 2′-O and 4′-C of the sugar moiety were bridged with the methylene chain and 3′-O was replaced by 3′-NH, on pyrimidine motif triplex formation at physiological pH. The modification not only significantly increased the thermal stability of the triplex but also increased the binding constant of triplex formation about 15-fold. The increased magnitude of the binding constant was not significantly changed when the number and position of the modification in TFO changed. The consideration of the observed thermodynamic parameters suggested that the increased rigidity of the modified TFO in the free state resulting from the bridging of different positions of the sugar moiety with an alkyl chain and the increased hydration of the modified TFO in the free state caused by the introduction of polar nitrogen atoms may significantly increase the binding constant at physiological pH. The study on the TFO viability in human serum showed that the modification significantly increased the resistance of TFO against nuclease degradation. This study presents an effective approach for designing novel chemically modified TFOs with higher binding affinity of triplex formation at physiological pH and higher nuclease resistance under physiological condition, which may eventually lead to progress in various triplex-formation-based strategies *in vivo*.

1. Introduction

In recent years, triplex nucleic acid has attracted considerable interest because of its possible biological functions *in vivo* and its wide variety of potential applications, such as artificial regulation of gene expression by antigene technology, mapping of genomic DNA, and gene-targeted mutagenesis [1–5]. A triplex nucleic acid is usually formed through the sequence-specific interaction of a single-stranded homopyrimidine or homopurine triplex-forming oligonucleotide (TFO) with the major groove of a homopurine–homopyrimidine stretch in duplex DNA [3,4]. In the pyrimidine motif triplex, a homopyrimidine TFO binds parallel to the homopurine strand of the target duplex by Hoogsteen hydrogen bonding to form T•A:T and C^+•G:C base triplets [3,4]. On the other hand, in the purine motif triplex, a homopurine TFO binds antiparallel to the homopurine strand of the target duplex by reverse Hoogsteen hydrogen bonding to form A•A:T (or T•A:T) and G•G:C base triplets [3,4].

Because protonation of the cytosine bases in a homopyrimidine TFO is required to enable binding with the guanine bases of the G:C target duplex, the formation of the pyrimidine motif triplex requires an environment with acidic pH, and is thus extremely unstable at physiological neutral pH [6–8]. On the other hand, the pH-independent formation of the purine motif triplex is possible at physiological neutral pH. However, purine motif triplex formation is severely inhibited by physiological concentrations of certain monovalent cations, especially K^+ ions [9,10]. The undefined association between K^+ and the guanine-rich homopurine TFO has been considered to explain this inhibitory effect [9,10]. Thus, the stabilization of the pyrimidine motif triplex at physiological neutral pH is necessary for improving its potential in various

Abbreviations: 3′-amino-2′,4′-BNA, 3′-amino-2′-*O*,4′-*C*-methylene bridged nucleic acid; CD, circular dichroism; EMSA, electrophoretic mobility shift assay; HPLC, high-performance liquid chromatography; ITC, isothermal titration calorimetry; TFO, triplex-forming oligonucleotide.

* Corresponding author. Tel.: +81 3 5228 8259; fax: +81 3 5261 4631.
E-mail address: htorigoe@rs.kagu.tus.ac.jp (H. Torigoe).

0300-9084/$ – see front matter © 2012 Elsevier Masson SAS. All rights reserved.
doi:10.1016/j.biochi.2012.01.003

triplex-formation-based strategies. Replacement of the cytosine bases in a homopyrimidine TFO with 5-methylcytosine [7,11–13] or other chemically modified base analogues [14–18], and conjugation of different DNA intercalators to TFO [19,20] have been used to overcome the requirement of an acidic pH for the pyrimidine motif triplex formation and to stabilize the pyrimidine motif triplex at physiological neutral pH.

We first synthesized and developed a new class of chemical modifications of nucleic acids, 3′-amino-2′-*O*,4′-*C*-methylene bridged nucleic acid (3′-amino-2′,4′-BNA) (Fig. 1a), in which 2′-O and 4′-C of the sugar moiety were bridged with the methylene chain, and 3′-O was replaced by 3′-NH [21,22]. The thermal stability of the triplex with 3′-amino-2′,4′-BNA modified TFO at physiological neutral pH was much higher than that with the corresponding natural phosphodiester TFO, which was shown by the UV melting of the dissociation of the triplex [21,22]. However, the formation of the triplex involving 3′-amino-2′,4′-BNA modified TFO at physiological neutral pH has not yet been well-characterized. To explore the possibility of the application of 3′-amino-2′,4′-BNA modified TFO to various triplex-formation-based strategies *in vivo*, the investigation of the formation of the triplex involving 3′-amino-2′,4′-BNA modified TFO at physiological neutral pH may be more important than that of the dissociation of the same triplex. In addition, the mechanistic explanation for the 3′-amino-2′,4′-BNA modification-mediated triplex stabilization at physiological neutral pH remains to be provided. Therefore, we have examined the effect of the 3′-amino-2′,4′-BNA modification of TFO on pyrimidine motif triplex formation with another base sequence at physiological neutral pH. The thermodynamic effect of the 3′-amino-2′,4′-BNA modification on the pyrimidine motif triplex formation between a 23-base pair homopurine-homopyrimidine target duplex (Pur23A•Pyr23T) (Fig. 1b) and its specific 15-mer unmodified homopyrimidine TFO (Pyr15T) (Fig. 1b) or each of 3′-amino-2′,4′-BNA modified homopyrimidine TFO (Pyr15BNANP7-1, Pyr15BNANP7-2, Pyr15BNANP5-1, and Pyr15BNANP5-2) (Fig. 1b) has been analyzed by the electrophoretic mobility shift assay (EMSA) [23–29], UV melting, and isothermal titration calorimetry (ITC) [24–26,28,30–33]. To examine the effect of the modified positions, Pyr15BNANP7-1 and Pyr15BNANP7-2 contain one modification every 2 nucleotides starting from the first and second positions at the 5′-terminal, respectively. Pyr15BNANP5-1 and Pyr15BNANP5-2 contain one modification every 3 nucleotides starting from the first and second positions at the 5′-terminal, respectively. To explore the possibility of the application of 3′-amino-2′,4′-BNA modified TFOs *in vivo*, the resistance of the unmodified and 3′-amino-2′,4′-BNA modified TFOs against nuclease degradation in human serum has been also investigated by native polyacrylamide gel electrophoresis and anion-exchange high-performance liquid chromatography (HPLC). We found that the 3′-amino-2′,4′-BNA modification of TFO increased the binding constant for the pyrimidine motif triplex formation at physiological neutral pH about 15-fold. We also observed that the nuclease resistance of the 3′-amino-2′,4′-BNA modified TFOs was significantly higher than that of the unmodified TFO. The mechanism of the 3′-amino-2′,4′-BNA modification to promote the pyrimidine motif triplex formation will be discussed. This information will present an effective approach for designing novel chemically modified TFOs with higher binding affinity of the pyrimidine motif triplex formation at physiological neutral pH.

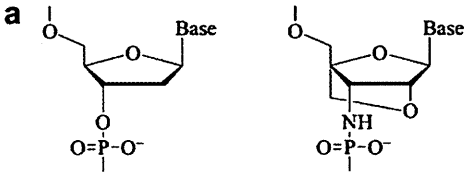

b

```
Pyr15T              5′-CTCTTCTTTTCTTTC-3′
Pyr15BNANP7-1       5′-CTCTTCTTTTCTTTC-3′
Pyr15BNANP7-2       5′-CTCTTCTTTTCTTTC-3′
Pyr15BNANP5-1       5′-CTCTTCTTTTCTTTC-3′
Pyr15BNANP5-2       5′-CTCTTCTTTTCTTTC-3′
Pur23A        5′-GCGCGAGAAGAAAAGAAAGCCGG-3′
Pyr23T        3′-CGCGCTCTTCTTTTCTTTCGGCC-5′
Pyr15NS             5′-TCTCCTCCCCTCCCT-3′
C: C with 3′-amino-2′-O,4′-C-methylene bridge
T: T with 3′-amino-2′-O,4′-C-methylene bridge
```

Fig. 1. (a) Structural formulas for phosphodiester (PO) and 3′-amino-2′-*O*,4′-*C*-methylene bridged nucleic acid (3′-amino-2′,4′-BNA)-modified backbones. (b) Oligonucleotide sequences for the target duplex (Pur23A•Pyr23T), the specific TFOs (Pyr15T, Pyr15BNANP7-1, Pyr15BNANP7-2, Pyr15BNANP5-1, and Pyr15BNANP5-2), and the nonspecific oligonucleotide (Pyr15NS).

2. Materials and methods

2.1. Preparation of oligonucleotides

We synthesized 23-mer complementary oligonucleotides for the target duplex, Pur23A and Pyr23T (Fig. 1b), a 15-mer unmodified homopyrimidine TFO specific to the target duplex, Pyr15T (Fig. 1b), and a 15-mer nonspecific homopyrimidine oligonucleotide, Pyr15NS (Fig. 1b), on an ABI DNA synthesizer using the solid-phase cyanoethyl phosphoramidite method; we then purified them by reverse-phase HPLC on a Wakosil DNA column. The 15-mer 3′-amino-2′,4′-BNA modified homopyrimidine TFOs specific to the target duplex, Pyr15BNANP7-1, Pyr15BNANP7-2, Pyr15BNANP5-1, and Pyr15BNANP5-2 (Fig. 1b), were synthesized and purified as described previously [21,22]. The concentration of all oligonucleotides was determined by UV absorbance. Complementary strands, Pur23A and Pyr23T, were annealed by heating up to 90 °C and then gradually cooling to room temperature. The annealed sample was applied to a hydroxyapatite column (BIORAD Inc.) to remove unpaired single strands. The concentration of the duplex DNA (Pur23A•Pyr23T) was determined by UV absorption, considering that an absorbance of 1 at 260 nm corresponds to a concentration of 50 μg/mL of DNA, with a M_r of 15180.

2.2. EMSA

EMSA experiments were performed as previously described, by 15% native polyacrylamide gel electrophoresis [24–29]. In a 9 μL aliquot of the reaction mixture, ^{32}P-labeled Pur23A•Pyr23T duplex (~1 nM) was mixed with increasing concentrations of the specific TFO (Pyr15T, Pyr15BNANP7-1, Pyr15BNANP7-2, Pyr15BNANP5-1, or Pyr15BNANP5-2) and the nonspecific oligonucleotide (Pyr15NS) in buffer [50 mM Tris-acetate (pH 7.0), 100 mM NaCl, and 10 mM $MgCl_2$]. Pyr15NS was added to achieve equimolar concentrations of TFO in each lane as well as to minimize the adhesion of the DNA (duplex and TFO) to plastic surfaces during incubation and subsequent losses during processing. After 6 h incubation at 37 °C, 2 μL of 50% glycerol solution containing bromophenol blue was added without changing the pH and salt concentrations of the reaction mixtures. Samples were then directly loaded onto a 15% native polyacrylamide gel prepared in buffer [50 mM Tris-acetate (pH 7.0) and 10 mM $MgCl_2$], and electrophoresis was performed at 8 V/cm for 16 h at 4 °C.

2.3. UV melting

UV melting experiments were carried out on a DU-640 spectrophotometer (Beckman Inc.) equipped with a Peltier-type cell holder. The cell path length was 1 cm. UV profiles were measured in buffer A (10 mM sodium cacodylate-cacodylic acid at pH 6.8 containing 200 mM NaCl and 20 mM $MgCl_2$) at a scan rate of 0.2 °C/min with detection at 260 nm for both melting and renaturing. The first derivative was calculated from the UV profiles. The peak temperature in the derivative curve was designated as the melting temperature, T_m. The triplex nucleic acid concentration used was 1 μM.

2.4. Circular dichroism (CD) spectroscopy

CD spectra at 20 °C were recorded in buffer A on a JASCO J-720 spectropolarimeter interfaced with a microcomputer. The cell path length was 1 cm. The triplex nucleic acid concentration used was 1 μM.

2.5. ITC

Isothermal titration experiments were carried out on a VP ITC system (Microcal Inc., U.S.A.) by following a previously described procedure [24–26,28]. The TFO and Pur23A•Pyr23T duplex solutions were prepared by extensive dialysis against buffer A or buffer B (10 mM sodium cacodylate-cacodylic acid at pH 5.8 containing 200 mM NaCl and 20 mM $MgCl_2$). The Pur23A•Pyr23T duplex solution in buffer A or buffer B was injected 20 times in 5 μL aliquots at 10 min intervals into the TFO solution without changing the reaction conditions. The heat of dilution of the injectant, which was measured by injecting the Pur23A•Pyr23T duplex solution into the same buffer, was subtracted from the heat of each injection. Each corrected heat value was divided by the number of moles of the Pur23A•Pyr23T duplex solution injected, and analyzed with Microcal Origin software supplied by the manufacturer.

2.6. Viability of TFO in human serum

Viability of TFO in human serum was examined by the following two procedures.

2.6.1. Analyses by native polyacrylamide gel electrophoresis

TFO was 5′-end labeled with ^{32}P using [γ-^{32}P] ATP and T4 polynucleotide kinase by using a standard procedure. An amount of 2 pmol of ^{32}P-labeled TFO was incubated at 37 °C in 200 μL of human serum from human male AB plasma (Sigma–Aldrich Co., USA). Aliquots of 5 μL were removed after 10, 20, 40, 60, and 120 min of incubation and mixed with 5 μL of stop solution (80% formamide, 50 mM EDTA) to terminate the reaction. The samples were loaded on 15% native polyacrylamide gels prepared in buffer [50 mM Tris-acetate (pH 7.0) and 100 mM $MgCl_2$], and electrophoresis was performed at 8 V/cm and 4 °C. The gels were scanned and analyzed by using a BAS system.

2.6.2. Analyses by anion-exchange HPLC

An amount of 1 nmol of TFO was incubated at 37 °C in 20 μL of 50% human serum from human male AB plasma (Sigma–Aldrich Co., USA). After incubation for 20, 60, and 120 min, each sample was mixed with 13 μL of formamide to terminate the reaction, and the samples were stored at −80 °C until HPLC analysis. The samples were mixed with 400 μL of HPLC buffer [25 mM Tris–HCl (pH 7.0) and 0.5% CH_3CN] and analyzed by anion-exchange HPLC on JASCO LC-2000 Plus series with detection at 260 nm by using a linear gradient of 0–0.5 M NH_4Cl in HPLC buffer over 45 min to resolve the products. The HPLC column used was TSK-GEL DNA-NPR (Tosoh, Japan). Under these conditions, peaks of all proteins from the human serum could be distinguished from those of the intact and degraded TFO. Degradation data from the acquired chromatograms were processed using ChromNAV software supplied by the manufacturer.

3. Results

3.1. Electrophoretic mobility shift assay of pyrimidine motif triplex formation at physiological neutral pH

The pyrimidine motif triplex formation of the target duplex (Pur23A•Pyr23T; Fig. 1b) with its specific unmodified (Pyr15T; Fig. 1b) or 3′-amino-2′,4′-BNA modified (Pyr15BNANP7-1, Pyr15BNANP7-2, Pyr15BNANP5-1, or Pyr15BNANP5-2; Fig. 1b) TFO was examined at pH 7.0 by EMSA (Fig. 2). Total oligonucleotide concentration ([specific TFO (Pyr15T, Pyr15BNANP7-1, Pyr15BNANP7-2, Pyr15BNANP5-1, or Pyr15BNANP5-2; Fig. 1b)] + [nonspecific oligonucleotide (Pyr15NS; Fig. 1b)]) was kept constant at 1 μM to minimize loss of DNA during processing and to assess sequence specificity. While incubation with 1 μM Pyr15NS alone did not cause a shift in the electrophoretic migration of the target duplex (see *lane 1* for Pyr15T), those with Pyr15T, Pyr15BNANP7-1, Pyr15BNANP7-2, Pyr15BNANP5-1, or Pyr15BNANP5-2 at particular concentrations caused retardation of the

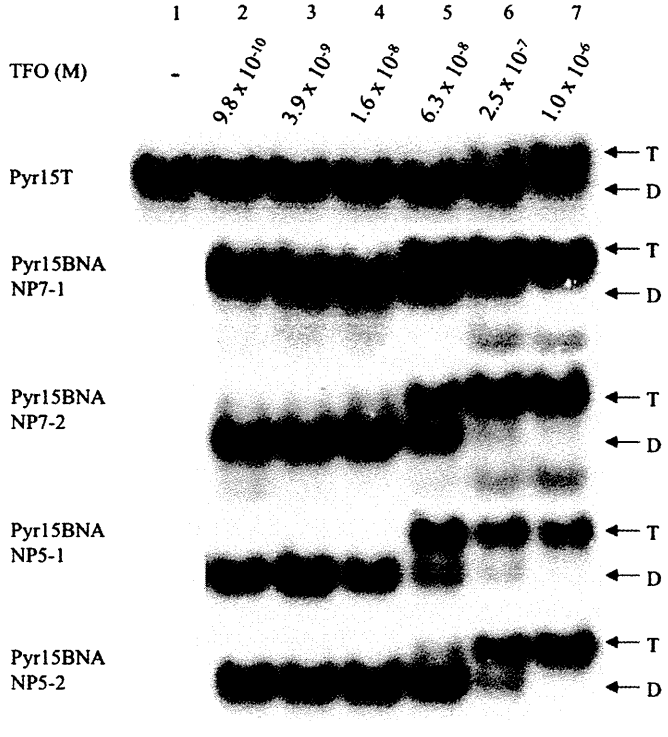

Fig. 2. EMSA of pyrimidine motif triplex formation using specific TFOs (Pyr15T, Pyr15BNANP7-1, Pyr15BNANP7-2, Pyr15BNANP5-1, or Pyr15BNANP5-2) at physiological neutral pH. Triplex formation was initiated by adding ^{32}P-labeled Pur23A•Pyr23T duplex (~1 nM) with the indicated final concentrations of the specific TFOs (Pyr15T, Pyr15BNANP7-1, Pyr15BNANP7-2, Pyr15BNANP5-1, or Pyr15BNANP5-2). The nonspecific oligonucleotide (Pyr15NS) was added to adjust to equimolar concentration (1 μM) of TFO (Pyr15T+Pyr15NS, Pyr15BNANP7-1+Pyr15NS, Pyr15BNANP7-2+Pyr15NS, Pyr15BNANP5-1+Pyr15NS, or Pyr15BNANP5-2+Pyr15NS) in each lane. Reaction mixtures involving Pyr15T, Pyr15BNANP7-1, Pyr15BNANP7-2, Pyr15BNANP5-1, or Pyr15BNANP5-2 in 50 mM Tris-acetate (pH 7.0), 100 mM NaCl, and 10 mM $MgCl_2$ were incubated for 6 h at 37 °C, and then electrophoretically separated at 4 °C on a 15% native polyacrylamide gel prepared in buffer [50 mM Tris-acetate (pH 7.0) and 10 mM $MgCl_2$]. Positions of the duplex (D) and triplex (T) are indicated.

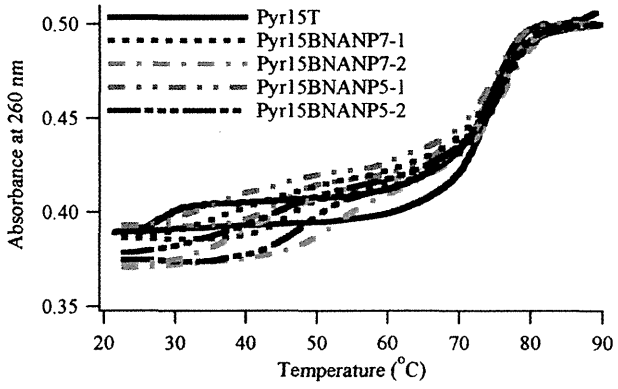

Fig. 3. UV profiles of pyrimidine motif triplexes formed with specific TFOs (Pyr15T, Pyr15BNANP7-1, Pyr15BNANP7-2, Pyr15BNANP5-1, or Pyr15BNANP5-2) for both melting and renaturing. The triplexes with Pyr15T, Pyr15BNANP7-1, Pyr15BNANP7-2, Pyr15BNANP5-1, or Pyr15BNANP5-2 in 10 mM sodium cacodylate-cacodylic acid (pH 6.8), 200 mM NaCl and 20 mM $MgCl_2$ were melted and renatured at a scan rate of 0.2 °C/min with detection at 260 nm. The cell path length was 1 cm. The triplex nucleic acid concentration used was 1 μM.

duplex migration owing to triplex formation [23]. The dissociation constant, K_d, of triplex formation was determined from the concentration of the TFO, which caused half of the target duplex to shift to the triplex [23]. K_d of the triplex with Pyr15T was estimated to be ~1 μM. In contrast, K_d of the triplex with each of the modified TFOs, Pyr15BNANP7-1, Pyr15BNANP7-2, Pyr15BNANP5-1, and Pyr15BNANP5-2 was ~0.06 μM, indicating that the 3′-amino-2′,4′-BNA modification of TFO increased the binding constant, K_a (= 1/K_d), of pyrimidine motif triplex formation at physiological neutral pH about 16-fold. The increase in K_a due to the modification was similar in magnitude among the four modified TFOs.

3.2. Spectroscopic characterization of pyrimidine motif triplex at physiological neutral pH

The thermal stability of the pyrimidine motif triplex with the unmodified or 3′-amino-2′,4′-BNA modified TFOs was investigated at pH 6.8 by UV profile for both melting and renaturing (Fig. 3 and Table 1). All the triplexes showed two-step transitions. The first transition at the lower temperature, T_{m1}, corresponded to the transition of the triplex to a duplex and a TFO, and the second transition at the higher temperature, T_{m2}, corresponded to the transition of the duplex to two single-strands (Fig. 3). The T_{m2} values were almost identical among all the triplexes (Table 1). Although a kind of irreversibility was observed for all TFOs [34], the T_{m1} values for the association and dissociation of Pyr15BNANP7-1, Pyr15BNANP7-2, Pyr15BNANP5-1, or Pyr15BNANP5-2 with the target duplex were significantly larger than that of Pyr15T in both the melting and renaturing curves (Table 1). These results

Table 1
Melting temperatures of the triplexes between a 23-base pair target duplex (Pur23A•Pyr23T) and a 15-mer TFO (Pyr15T, Pyr15BNANP7-1, Pyr15BNANP7-2, Pyr15BNANP5-1, or Pyr15BNANP5-2) in 10 mM sodium cacodylate-cacodylic acid (pH 6.8), 200 mM NaCl and 20 mM $MgCl_2$ for both melting and renaturing.

TFO	T_{m1} (°C) melting	T_{m1} (°C) renaturing	T_{m2} (°C) melting	T_{m2} (°C) renaturing
Pyr15T	28.5 ± 0.2	23.1 ± 0.5	73.5 ± 0.1	72.9 ± 0.3
Pyr15BNANP7-1	53.3 ± 0.1	45.3 ± 0.2	73.5 ± 0.1	73.4 ± 0.1
Pyr15BNANP7-2	53.3 ± 0.1	44.7 ± 0.1	73.5 ± 0.3	73.9 ± 0.1
Pyr15BNANP5-1	50.3 ± 0.1	45.7 ± 0.1	73.5 ± 0.2	73.3 ± 0.3
Pyr15BNANP5-2	52.2 ± 0.5	45.2 ± 0.1	72.9 ± 0.3	73.9 ± 0.2

demonstrate that the thermal stability of the triplexes with 3′-amino-2′,4′-BNA modified TFO was significantly higher than that with the unmodified TFO, confirming our previous result [21,22] that the 3′-amino-2′,4′-BNA modification of TFO increased the thermal stability of the pyrimidine motif triplex at physiological neutral pH. In addition, we examined the temperature dependence of the absorbance at 295 nm for the triplexes involving unmodified or 3′-amino-2′,4′-BNA modified TFOs to follow the deprotonation and protonation of the cytosines in triplex denaturation and formation (Figure S1 in Supplementary Material) [35]. Although the change of the absorbance at 295 nm during temperature shift was significantly smaller than that at 260 nm, the temperature range of deprotonation and protonation of the cytosines for Pyr15BNANP7-1, Pyr15BNANP7-2, Pyr15BNANP5-1, or Pyr15BNANP5-2 was higher than that for Pyr15T in spite of a kind of irreversibility for all TFOs (Figure S1 in Supplementary Material).

To further characterize the triplexes involving the unmodified or 3′-amino-2′,4′-BNA modified TFOs, CD spectra of the triplexes were measured at 20 °C and pH 6.8 (Fig. 4). The overall shape of the CD spectra was similar among all the profiles. A significant negative band in the short-wavelength (210–220 nm) region was observed in all the profiles, confirming triplex formation involving each TFO [36]. The intensity of the negative short-wavelength (210–220 nm) band for the triplexes involving each of the modified TFOs, Pyr15BNANP7-1, Pyr15BNANP7-2, Pyr15BNANP5-1, and Pyr15BNANP5-2 was larger than that observed for the triplex involving Pyr15T, indicating that all the triplexes involving the 3′-amino-2′,4′-BNA modified TFO had more features of the A-like conformation than that involving the unmodified TFO [37].

3.3. Thermodynamic analyses of pyrimidine motif triplex formation by ITC

We examined the thermodynamic parameters of the pyrimidine motif triplex formation between a 23-base pair target duplex (Pur23A•Pyr23T) and its specific 15-mer unmodified (Pyr15T) or 3′-amino-2′,4′-BNA modified (Pyr15BNANP7-1, Pyr15BNANP7-2, Pyr15BNANP5-1, or Pyr15BNANP5-2) TFO at 25 °C and pH 6.8 by ITC. To investigate the pH dependence of the pyrimidine motif triplex formation, the thermodynamic parameters of the triplex formation between Pur23A•Pyr23T and Pyr15T were also analyzed at 25 °C and pH 5.8 by ITC. Fig. 5a shows a typical ITC profile for the triplex formation between Pyr15BNANP7-1 and Pur23A•Pyr23T at

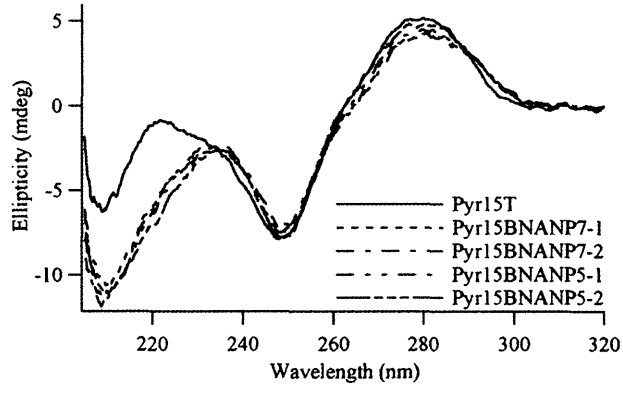

Fig. 4. CD spectra of pyrimidine motif triplexes formed with specific TFOs (Pyr15T, Pyr15BNANP7-1, Pyr15BNANP7-2, Pyr15BNANP5-1, or Pyr15BNANP5-2). The triplexes with Pyr15T, Pyr15BNANP7-1, Pyr15BNANP7-2, Pyr15BNANP5-1, or Pyr15BNANP5-2 in 10 mM sodium cacodylate-cacodylic acid (pH 6.8), 200 mM NaCl and 20 mM $MgCl_2$ were measured at 20 °C in the wavelength range of 205–320 nm. The cell path length was 1 cm. The triplex nucleic acid concentration used was 1 μM.

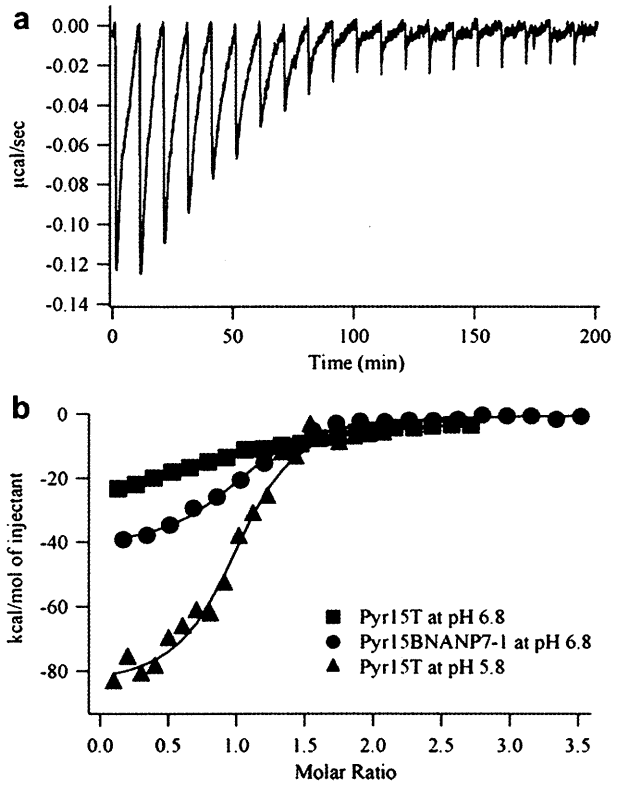

Fig. 5. Thermodynamic analyses of pyrimidine motif triplex formation using Pyr15T or Pyr15BNANP7-1 at pH 6.8, and Pyr15T at pH 5.8 by ITC. (a) Typical ITC profiles for the triplex formation between Pyr15BNANP7-1 and Pur23A•Pyr23T at 25 °C and pH 6.8. Pur23A•Pyr23T solution (140 μM) in 10 mM sodium cacodylate-cacodylic acid (pH 6.8), 200 mM NaCl and 20 mM $MgCl_2$ was injected 20 times in 5 μL aliquots into 3.0 μM Pyr15BNANP7-1 solution, which was dialyzed against the same buffer. Aliquots were injected over 12 s at 10 min intervals. (b) Titration plots as a function of the molar ratio [Pur23A•Pyr23T]/[TFO]. The data were fitted by a nonlinear least-squares method.

25 °C and pH 6.8. An exothermic heat pulse was observed after each injection of Pur23A•Pyr23T into Pyr15BNANP7-1. The magnitude of each peak decreased gradually with each new injection, and a small peak was still observed at the molar ratio corresponding to the last injection. The area of the small peak was equal to the heat of dilution measured in a separate experiment by injecting Pur23A•Pyr23T into the same buffer. The area under each peak was integrated, and the heat of dilution of Pur23A•Pyr23T was subtracted from the integrated values. The corrected heat value was divided by the moles of injected solution, and the resulting values were plotted as a function of the molar ratio of [Pur23A•Pyr23T]/[Pyr15BNANP7-1], as shown in Fig. 5b. A sigmoidal curve was fitted to the resultant titration plot by a nonlinear least-squares method. The binding constant, K_a, and the enthalpy change, ΔH, were obtained from the fitted curve [32]. The Gibbs free energy change, ΔG, and the entropy change, ΔS, were calculated from the equation, $\Delta G = -RT\ln K_a = \Delta H - T\Delta S$, where R is the gas constant and T is the temperature [32]. The titration plots for Pyr15T at pH 6.8 and pH 5.8 are also shown in Fig. 5b. The thermodynamic parameters for Pyr15T at pH 6.8 and pH 5.8 were obtained from the titration plots in the same way. The ITC profiles and the titration plots for Pyr15BNANP7-2, Pyr15BNANP5-1, and Pyr15BNANP5-2 at pH 6.8 were almost the same as those observed for Pyr15BNANP7-1 at pH 6.8. The thermodynamic parameters for Pyr15BNANP7-2, Pyr15BNANP5-1, and Pyr15BNANP5-2 at pH 6.8 were obtained from the titration plots in the same way.

Table 2 summarizes the thermodynamic parameters for the formation of pyrimidine motif triplexes with Pyr15T, Pyr15BNANP7-1, Pyr15BNANP7-2, Pyr15BNANP5-1, and Pyr15BNANP5-2 at 25 °C and pH 6.8 and for the formation with Pyr15T at 25 °C and pH 5.8, obtained from ITC. The signs of both ΔH and ΔS were negative under each condition. Because an observed negative ΔS was unfavorable for triplex formation, triplex formation was driven by a large negative ΔH under each condition. K_a for Pyr15T at pH 5.8 was about 20-fold larger than that observed for Pyr15T at pH 6.8, confirming, like others [6–8], that physiological neutral pH is unfavorable for the pyrimidine motif triplex formation involving C^+•G:C triads. In addition, K_a for each of the 3′-amino-2′,4′-BNA modified TFOs at pH 6.8 was about 15-fold larger than that observed for Pyr15T at pH 6.8, indicating that the 3′-amino-2′,4′-BNA modification of TFO increased K_a for the pyrimidine motif triplex formation at physiological neutral pH, which is consistent with the results of EMSA (Fig. 2). The increase in K_a due to TFO modification was similar in magnitude among the four modified TFOs. Further, although the K_a and ΔG values for triplex formation with each of the modified TFOs at pH 6.8 and with Pyr15T at pH 5.8 were quite similar, the components of ΔG, that is, ΔH and ΔS, obviously differed in value (Table 2). The absolute values of the negative ΔH and ΔS for each of the modified TFOs at pH 6.8 were significantly smaller than those observed for Pyr15T at pH 5.8 (Table 2).

To examine the significance of 3′-amino modification in the 3′-amino-2′,4′-BNA modification, we investigated thermodynamic parameters for the triplex formation involving 2′,4′-BNA modified TFOs at pH 6.8 by ITC (Table S1 in Supplementary Material). The positions of 2′,4′-BNA modification were the same as those of 3′-amino-2′,4′-BNA modification. K_a for 2′,4′-BNA modified TFOs at pH 6.8 was about 4-fold larger than that observed for Pyr15T at pH 6.8 (Table S1 in Supplementary Material). On the other hand, K_a for 3′-amino-2′,4′-BNA modified TFOs at pH 6.8 was about 15-fold larger than that observed for Pyr15T at pH 6.8 (Table 2). Thus, K_a at pH 6.8 promoted by 2′,4′-BNA modification was significantly further increased by 3′-amino modification. 3′-amino modification significantly contributes to enhancement of the pyrimidine motif triplex formation at physiological neutral pH.

To examine the generality of the effect of 3′-amino-2′,4′-BNA modification to promote pyrimidine motif triplex formation at physiological neutral pH, we investigated thermodynamic

Table 2
Thermodynamic parameters for the triplex formation between a 23-base pair target duplex (Pur23A•Pyr23T) and a 15-mer TFO (Pyr15T, Pyr15BNANP7-1, Pyr15BNANP7-2, Pyr15BNANP5-1, or Pyr15BNANP5-2) at 25 °C, obtained from ITC.

TFO	pH	K_a (M^{-1})	K_a (relative)	ΔG (kcal mol^{-1})	ΔH (kcal mol^{-1})	ΔS (cal mol^{-1} K^{-1})
Pyr15T	5.8[a]	$(3.83 \pm 0.74) \times 10^6$	19.4	−8.98 ± 0.13	−85.6 ± 2.6	−257 ± 9.1
Pyr15T	6.8[b]	$(1.97 \pm 0.43) \times 10^5$	1.0	−7.22 ± 0.15	−34.9 ± 2.2	−92.7 ± 8.0
Pyr15BNANP7-1	6.8[b]	$(2.43 \pm 0.39) \times 10^6$	12.3	−8.71 ± 0.10	−48.3 ± 2.0	−133 ± 6.9
Pyr15BNANP7-2	6.8[b]	$(2.52 \pm 0.51) \times 10^6$	12.8	−8.73 ± 0.14	−56.4 ± 3.3	−160 ± 11.4
Pyr15BNANP5-1	6.8[b]	$(2.43 \pm 0.18) \times 10^6$	12.3	−8.71 ± 0.05	−48.3 ± 3.1	−133 ± 10.6
Pyr15BNANP5-2	6.8[b]	$(2.98 \pm 0.48) \times 10^6$	15.1	−8.83 ± 0.10	−53.2 ± 2.6	−149 ± 9.0

[a] 10 mM sodium cacodylate-cacodylic acid (pH 5.8), 200 mM NaCl and 20 mM $MgCl_2$.
[b] 10 mM sodium cacodylate-cacodylic acid (pH 6.8), 200 mM NaCl and 20 mM $MgCl_2$.

parameters for the triplex formation with another base sequence between 21-bp target duplex and each of 15-mer unmodified or 3′-amino-2′,4′-BNA modified TFO (Table S2 in Supplementary Material). Only one 3′-amino-2′,4′-BNA modification was introduced just in the middle of 15-mer TFO. K_a for the 3′-amino-2′,4′-BNA modified TFO at pH 7.0 was significantly larger than that observed for the unmodified TFO at pH 7.0, indicating that even only one 3′-amino-2′,4′-BNA modification of TFO increased K_a for the pyrimidine motif triplex formation at physiological neutral pH, which is consistent with the results of Table 2.

3.4. Viability of TFOs in human serum against nuclease degradation

A major difficulty associated with the use of oligonucleotides as *in vivo* agents is their rapid degradation by nuclease *in vivo* [38]. To explore the possibility of the use of 3′-amino-2′,4′-BNA modified TFOs in various triplex-formation-based strategies *in vivo*, we examined the resistance of the unmodified or 3′-amino-2′,4′-BNA modified TFOs to nuclease degradation. The series of TFOs 5′-end labeled with ^{32}P were incubated at 37 °C in human serum, and their degradation was assessed by 15% native polyacrylamide gel electrophoresis (Figure S2 in Supplementary Material). The entire Pyr15T was degraded and converted to shorter oligonucleotides within 10 min of incubation. In contrast, most of Pyr15BNANP7-2 and Pyr15BNANP5-2 remained intact even after 120 min of incubation. These results indicate that the 3′-amino-2′,4′-BNA modification contributed to an increase in the viability of TFOs in human serum. Because Pyr15BNANP7-1 and Pyr15BNANP5-1 containing the 3′-amino-2′,4′-BNA modification at the 5′-end could not be labeled with ^{32}P by T4 polynucleotide kinase, it was impossible to examine the resistance of Pyr15BNANP7-1 and Pyr15BNANP5-1 in human serum. Thus, to investigate the resistance of all TFOs, including Pyr15BNANP7-1 and Pyr15BNANP5-1, against nuclease degradation, their degradation was estimated by anion-exchange HPLC after incubating the TFOs at 37 °C in human serum. Fig. 6 shows the percentage of intact oligonucleotides as a function of the incubation time. Only 20% of intact Pyr15T was detected after 20 min of incubation with human serum, and Pyr15T was completely degraded within 60 min. On the other hand, more than 50% of each of the 3′-amino-2′,4′-BNA modified TFOs remained intact even after 120 min of incubation with human serum. These results indicate that the 3′-amino-2′,4′-BNA modification significantly increased the nuclease resistance of TFOs in human serum. The results of anion-exchange HPLC are consistent with those of native polyacrylamide gel electrophoresis (Figure S2 in Supplementary Material).

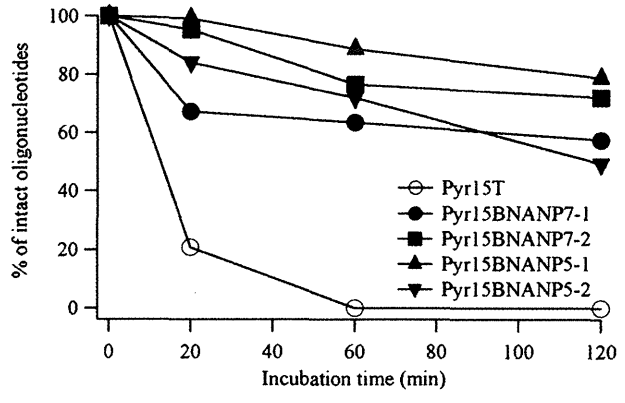

Fig. 6. Viability of specific TFOs (Pyr15T, Pyr15BNANP7-1, Pyr15BNANP7-2, Pyr15BNANP5-1, and Pyr15BNANP5-2) in human serum. TFOs (1 nmol) were incubated in human serum at 37 °C, and aliquots were removed at the time points indicated and analyzed by anion-exchange HPLC. The percentage of intact oligonucleotides was determined and plotted as a function of the incubation time.

4. Discussion

K_a of the pyrimidine motif triplex formation with Pyr15T at pH 5.8 was about 20-fold larger than that observed with Pyr15T at pH 6.8 (Table 2), which is consistent with the previously reported results that physiological neutral pH is unfavorable for pyrimidine motif triplex formation involving C^+·G:C triads [6–8]. On the other hand, K_a of the pyrimidine motif triplex formation with each of the 3′-amino-2′,4′-BNA modified TFOs at pH 6.8 was about 15-fold larger than that observed with Pyr15T at pH 6.8 (Table 2). The increase in K_a at physiological neutral pH by the modification of TFO was supported by the results of EMSA (Fig. 2). Although the magnitudes of K_d ($=1/K_a$) were different between EMSA (Fig. 2) and ITC (Table 2) due to the difference in the experimental buffer conditions, the modification of TFO promoted the pyrimidine motif triplex formation in both buffer conditions. In addition, the modification of TFO increased the thermal stability of the pyrimidine motif triplexes at physiological neutral pH (Fig. 3 and Table 1), which confirmed our previous results [21,22]. These results indicate that the 3′-amino-2′,4′-BNA modification of TFO promotes the pyrimidine motif triplex formation at physiological neutral pH. The 3′-amino-2′,4′-BNA modification of TFO may promote the assembly of the 3′-amino-2′,4′-BNA modified TFO and the target duplex, which may enhance protonation of cytosine bases of the 3′-amino-2′,4′-BNA modified TFO to form the triplex. The pK_a increase of cytosine bases of the 3′-amino-2′,4′-BNA modified TFO in the triplex may be caused by the intrinsic stability of the triplex involving the 3′-amino-2′,4′-BNA modified TFO.

Because the formed triplex structures involving Pyr15T at pH 5.8 and Pyr15T at pH 6.8 are the same, the absolute values of ΔH and ΔS involved in the triplex formation measured by ITC could in fact be the same for the two conditions. However, the absolute values of ΔH and ΔS for Pyr15T at pH 6.8 were significantly smaller than those observed for Pyr15T at pH 5.8. When ΔH and ΔS are calculated from the fitting procedure of ITC, the value of the heat observed by ITC is divided not by the effective concentration really involved in the triplex formation, but by the apparent concentration added to the triplex formation [32]. The calculation does not take into consideration what percentage of the added concentration is actually effectively involved in the triplex formation. Thus, if the triplex formation is substoichiometric under a certain condition, the absolute values of ΔH and ΔS estimated by ITC are smaller than those observed for the more stoichiometric triplex formation under another condition. Therefore, the significantly smaller absolute values of ΔH and ΔS for Pyr15T at pH 6.8 relative to those for Pyr15T at pH 5.8 (Table 2) suggest that the triplex formation with Pyr15T at pH 6.8 was significantly more substoichiometric than that with Pyr15T at pH 5.8. This was also supported by the significantly smaller absolute values of K_a and ΔG for Pyr15T at pH 6.8 (Table 2). In contrast, the K_a and ΔG values for Pyr15T at pH 5.8 and those for the 3′-amino-2′,4′-BNA modified TFOs at pH 6.8 were quite similar (Table 2), suggesting that the triplex formations under these conditions were similarly quite stoichiometric. We conclude that the triplex formation with Pyr15T at pH 6.8 was significantly more substoichiometric than that with Pyr15T at pH 5.8 and that with the 3′-amino-2′,4′-BNA modified TFOs at pH 6.8. Thus, to discuss the mechanism for promotion of triplex formation by 3′-amino-2′,4′-BNA modification of TFO, the comparison between the values of ΔH and ΔS observed for Pyr15T at pH 6.8 and those for the modified TFOs at pH 6.8 is not valid due to the significantly lower stoichiometry for Pyr15T at pH 6.8. The comparison between the values of ΔH and ΔS for Pyr15T at pH 5.8 and those for modified TFOs at pH

6.8 with similar stoichiometry will indicate a reasonable mechanism for the promotion of triplex formation by the modification of TFO, as discussed below.

Although the values of K_a and ΔG for Pyr15T at pH 5.8 and those for the 3′-amino-2′,4′-BNA modified TFOs at pH 6.8 were quite similar (Table 2), the components of ΔG, that is, ΔH and ΔS, were obviously different in value. The absolute values of the negative ΔH and ΔS for the modified TFOs at pH 6.8 were smaller than those observed for Pyr15T at pH 5.8 (Table 2). The observed negative ΔH upon triplex formation, measured by ITC, reflects a major contribution from the hydrogen bonding and the base stacking involved in triplex formation [39–42]. The immobilization of electrostricted water molecules around polar atoms upon triplex formation is also considered to be a major contributor to the observed negative ΔH of triplex formation [39–42]. The value of ΔH also includes a contribution from the protonation of cytosine bases upon hydrogen bonding, and the accompanying deprotonation of the cacodylate buffer releasing protons to bind with the cytosine bases [43]. Because the degree of protonation may be similar between the modified TFOs at pH 6.8 and Pyr15T at pH 5.8 because of the similarity of stoichiometry discussed above, and as the protons that bind with the cytosine bases are released from the same cacodylate buffer in both cases, the values of ΔH derived from the protonation of the cytosine bases and the accompanying deprotonation of the cacodylate buffer should be similar in the two cases. Thus, the difference in ΔH of formation between the stoichiometric triplexes with modified TFOs at pH 6.8 and Pyr15T at pH 5.8 (Table 2) suggests that the hydrogen bonding and/or the base stacking in the triplexes with modified TFO and the degree of immobilization of water molecules around the protonated cytosine bases and polar nitrogen atoms of the triplexes with the modified TFO may be significantly different from that with the corresponding unmodified TFO. In fact, the CD spectra show that the triplexes with 3′-amino-2′,4′-BNA modified TFO had more features of the A-like conformation than that with the corresponding unmodified TFO (Fig. 4) [37]. The A-like conformation obtained by the modification of TFO may result in the difference in the negative ΔH between the unmodified and modified TFOs. On the other hand, contributions to ΔS observed upon triplex formation measured by ITC mainly come from two factors: a negative conformational entropy change from the conformational restraint of the TFO involved in triplex formation and a positive dehydration entropy change resulting from the release of structured water molecules surrounding the TFO and the target duplex upon triplex formation [39–42]. Therefore, one of the reasons for the smaller magnitude of the negative ΔS for the 3′-amino-2′,4′-BNA modified TFOs at pH 6.8 in comparison with that for Pyr15T at pH 5.8 (Table 2) may be a result of the negative conformational entropy change. The 3′-amino-2′,4′-BNA modified TFO in the free state may be more rigid than the corresponding unmodified TFO, because the 2′-O and 4′-C positions of the sugar moiety of the 3′-amino-2′,4′-BNA are bridged with a methylene chain. The increased rigidity of the modified TFO in the free state relative to the corresponding unmodified TFO may lead to a smaller loss of conformational entropy upon triplex formation in the case of the modified TFO at physiological neutral pH. Another reason for the smaller magnitudes of the negative ΔS for the 3′-amino-2′,4′-BNA modified TFOs at pH 6.8 relative to that for Pyr15T at pH 5.8 (Table 2) may be inferred from the positive dehydration entropy change. Previous studies on crystallographic structures [44] and molecular dynamics simulation [45,46] showed that the degree of hydration around the N3′-phosphoramidate backbone was enhanced in comparison with that around the corresponding DNA phosphodiester backbone. The increased hydration of the modified TFO in the free state relative to the corresponding unmodified TFO may cause a larger gain of dehydration entropy upon triplex formation with the modified TFO at physiological neutral pH. These two possible reasons, the smaller loss of conformational entropy and the larger gain of dehydration entropy, may account for the smaller magnitudes of the negative ΔS observed for the modified TFOs at pH 6.8. This provides a favorable component to ΔG and leads to the increase in K_a of triplex formation at physiological neutral pH. In conclusion, because the smaller absolute values of the negative ΔH for the modified TFOs at pH 6.8 in comparison with that for Pyr15T at pH 5.8 were unfavorable for promotion of triplex formation (Table 2), the hydrogen bonding and the base stacking, which are major contributions to the observed ΔH upon triplex formation, cannot be major factors contributing to promote the pyrimidine motif triplex formation at physiological neutral pH. On the other hand, because the smaller absolute values of the negative ΔS for the modified TFOs at pH 6.8 in comparison with that for Pyr15T at pH 5.8 were favorable for promotion of triplex formation (Table 2), the increased rigidity and the increased hydration of the modified TFO in the free state, which are major contributions to the observed ΔS upon triplex formation, are major factors contributing to the increase in K_a of the pyrimidine motif triplex formation at physiological neutral pH.

The increase in K_a by the 3′-amino-2′,4′-BNA modification was similar in magnitude among the four modified TFOs (Fig. 2 and Table 2), indicating that the number and position of the modification did not significantly affect the magnitude of increase in K_a at physiological neutral pH. The increased rigidity and hydration of the modified TFO may be more important than the variation of the number and position of the modification in achieving the increase in K_a of the pyrimidine motif triplex formation at physiological neutral pH. Thus, other modification strategies to achieve increased rigidity and hydration of TFO may also be useful to increase K_a of the pyrimidine motif triplex formation at physiological neutral pH.

The nuclease resistance of 3′-amino-2′,4′-BNA modified TFO was significantly higher than that of the unmodified TFO (Fig. 6 and Figure S2 in Supplementary Material). The modification increased the nuclease resistance of TFOs in human serum. Previously, the nuclease resistance of the phosphorothioate backbone, in which a nonbridging oxygen of a phosphodiester group was replaced by a sulfur atom, was known to be significantly higher than that of the unmodified backbone [47,48]. However, K_a of triplex formation with the phosphorothioate modified TFO was significantly smaller than that with the unmodified TFO [33,49]. Thus, the phosphorothioate modification increased the nuclease resistance of TFO, but it decreased the triplex forming ability. On the other hand, as discussed above, the 3′-amino-2′,4′-BNA modification of TFO increased the pyrimidine motif triplex forming ability at physiological neutral pH (Fig. 2 and Table 2). Therefore, the 3′-amino-2′,4′-BNA modification enhanced both the nuclease resistance of TFO and the pyrimidine motif triplex forming ability at physiological neutral pH. We conclude that due to these excellent properties 3′-amino-2′,4′-BNA modification may be more favorable than phosphorothioate modification upon application of TFO to various pyrimidine motif triplex-formation-based strategies *in vivo*.

5. Conclusions

The present study has clearly demonstrated that the 3′-amino-2′,4′-BNA modification of TFO promoted pyrimidine motif triplex formation at physiological neutral pH. It has also shown that the modification of TFO increased the nuclease resistance of TFO in human serum. Our results certainly support the idea that the 3′-amino-2′,4′-BNA modified oligonucleotides may have the potential to be applied to various pyrimidine motif triplex-formation-based strategies, such as artificial regulation of gene expression by antigene technology, mapping of genomic DNA, and gene-targeted

mutagenesis. In addition, the present study has shown that the increased rigidity and the increased hydration of the modified TFO in the free state may enable the significant increase in K_a for the pyrimidine motif triplex formation at physiological neutral pH. We conclude that the design of TFO, involving the bridging of different positions of the sugar moiety with an alkyl chain for increased rigidity and the introduction of polar nitrogen atoms for increased hydration, is certainly promising for the promotion of pyrimidine motif triplex formation at physiological neutral pH, which may eventually lead to progress in various pyrimidine motif triplex-formation-based strategies.

Acknowledgments

This work was supported in part by a Grant-in-Aid for Scientific Research on Innovative Areas (22113519 to H.T.), Grant-in-Aid for Exploratory Research (20655038 to S. O.), Grant-in-Aid for Scientific Research (B) (21350094 to S.O.), and Grant-in-Aid for JSPS Fellows (22-10383 to K.S.) from the Ministry of Education, Science, Sports, and Culture of Japan. This work was also supported partly by the Program for Promotion of Fundamental Studies in Health Sciences of the National Institute of Biomedical Innovation (NIBIO).

Appendix. Supplementary data

Supplementary data associated with this article can be found, in the online version, at doi:10.1016/j.biochi.2012.01.003.

References

[1] J.Y. Chin, E.B. Schleifman, P.M. Glazer, Repair and recombination induced by triple helix DNA, Front. Biosci. 12 (2007) 4288–4297.
[2] J.J. Bissler, Triplex DNA and human disease, Front. Biosci. 12 (2007) 4536–4546.
[3] M. Duca, P. Vekhoff, K. Oussedik, L. Halby, P.B. Arimondo, The triple helix: 50 years later, the outcome, Nucleic Acids Res. 36 (2008) 5123–5138.
[4] A. Jain, G. Wang, K.M. Vasquez, DNA triple helices: biological consequences and therapeutic potential, Biochimie 90 (2008) 1117–1130.
[5] R.D. Wells, DNA triplexes and Friedreich ataxia, Faseb J. 22 (2008) 1625–1634.
[6] M.D. Frank-Kamenetskii, Protonated DNA structures, Methods Enzymol. 211 (1992) 180–191.
[7] S.F. Singleton, P.B. Dervan, Influence of pH on the equilibrium association constants for oligodeoxyribonucleotide-directed triple helix formation at single DNA sites, Biochemistry 31 (1992) 10995–11003.
[8] H. Shindo, H. Torigoe, A. Sarai, Thermodynamic and kinetic studies of DNA triplex formation of an oligohomopyrimidine and a matched duplex by filter binding assay, Biochemistry 32 (1993) 8963–8969.
[9] J.F. Milligan, S.H. Krawczyk, S. Wadwani, M.D. Matteucci, An anti-parallel triple helix motif with oligodeoxynucleotides containing 2'-deoxyguanosine and 7-deaza-2'-deoxyxanthosine, Nucleic Acids Res. 21 (1993) 327–333.
[10] A.J. Cheng, M.W. Van Dyke, Monovalent cation effects on intermolecular purine-purine-pyrimidine triple-helix formation, Nucleic Acids Res. 21 (1993) 5630–5635.
[11] J.S. Lee, M.L. Woodsworth, L.J. Latimer, A.R. Morgan, Poly(pyrimidine). poly(-purine) synthetic DNAs containing 5-methylcytosine form stable triplexes at neutral pH, Nucleic Acids Res. 12 (1984) 6603–6614.
[12] T.J. Povsic, P.B. Dervan, Triple helix formation by oligonucleotides on DNA Extended to the physiological Ph range, J. Am. Chem. Soc. 111 (1989) 3059–3061.
[13] L.E. Xodo, G. Manzini, F. Quadrifoglio, G.A. van der Marel, J.H. van Boom, Effect of 5-methylcytosine on the stability of triple-stranded DNA–a thermodynamic study, Nucleic Acids Res. 19 (1991) 5625–5631.
[14] A. Ono, P.O.P. Tso, L.S. Kan, Triplex formation of oligonucleotides containing 2'-O-Methylpseudoisocytidine in Substitution for 2'-Deoxycytidine, J. Am. Chem. Soc. 113 (1991) 4032–4033.
[15] S.H. Krawczyk, J.F. Milligan, S. Wadwani, C. Moulds, B.C. Froehler, M.D. Matteucci, Oligonucleotide-mediated triple helix formation using an N3-protonated deoxycytidine analog exhibiting pH-independent binding within the physiological range, Proc. Natl. Acad. Sci. U S A 89 (1992) 3761–3764.
[16] J.S. Koh, P.B. Dervan, Design of a Nonnatural Deoxyribonucleoside for Recognition of Gc base-pairs by oligonucleotide-directed triple helix formation, J. Am. Chem. Soc. 114 (1992) 1470–1478.
[17] M.C. Jetter, F.W. Hobbs, 7,8-Dihydro-8-oxoadenine as a replacement for cytosine in the third strand of triple helices. Triplex formation without hypochromicity, Biochemistry 32 (1993) 3249–3254.
[18] Y. Ueno, M. Mikawa, A. Matsuda, Nucleosides and nucleotides. 170. Synthesis and properties of oligodeoxynucleotides containing 5-[N-[2-[N, N-bis(2-aminoethyl)- amino]ethyl]carbamoyl]-2'-deoxyuridine and 5-[N-[3-[N, N-bis(3-aminopropyl) amino]propyl]carbamoyl]-2'-deoxyuridine, Bioconjug. Chem. 9 (1998) 33–39.
[19] J.S. Sun, C. Giovannangeli, J.C. Francois, R. Kurfurst, T. Montenay-Garestier, U. Asseline, T. Saison-Behmoaras, N.T. Thuong, C. Helene, Triple-helix formation by alpha oligodeoxynucleotides and alpha oligodeoxynucleotide-intercalator conjugates, Proc. Natl. Acad. Sci. U S A 88 (1991) 6023–6027.
[20] J.F. Mouscadet, C. Ketterle, H. Goulaouic, S. Carteau, F. Subra, M. Le Bret, C. Auclair, Triple helix formation with short oligonucleotide-intercalator conjugates matching the HIV-1 U3 LTR end sequence, Biochemistry 33 (1994) 4187–4196.
[21] S. Obika, M. Onoda, K. Morita, J. Andoh, M. Koizumi, T. Imanishi, 3'-amino-2',4'-BNA: novel bridged nucleic acids having an N3'->P5' phosphoramidate linkage, Chem. Commun. (Camb) (2001) 1992–1993.
[22] S. Obika, S.M. Rahman, B. Song, M. Onoda, M. Koizumi, K. Morita, T. Imanishi, Synthesis and properties of 3'-amino-2',4'-BNA, a bridged nucleic acid with a N3'->P5' phosphoramidate linkage, Bioorg. Med. Chem. 16 (2008) 9230–9237.
[23] V.I. Lyamichev, S.M. Mirkin, M.D. Frank-Kamenetskii, C.R. Cantor, A stable complex between homopyrimidine oligomers and the homologous regions of duplex DNAs, Nucleic Acids Res. 16 (1988) 2165–2178.
[24] H. Torigoe, A. Ferdous, H. Watanabe, T. Akaike, A. Maruyama, Poly(L-lysine)-graft-dextran copolymer promotes pyrimidine motif triplex DNA formation at physiological pH – thermodynamic and kinetic studies, J. Biol. Chem. 274 (1999) 6161–6167.
[25] H. Torigoe, Y. Hari, M. Sekiguchi, S. Obika, T. Imanishi, 2'-O,4'-C-methylene bridged nucleic acid modification promotes pyrimidine motif triplex DNA formation at physiological pH: thermodynamic and kinetic studies, J. Biol. Chem. 276 (2001) 2354–2360.
[26] H. Torigoe, Thermodynamic and kinetic effects of N3'->P5' phosphoramidate modification on pyrimidine motif triplex DNA formation, Biochemistry 40 (2001) 1063–1069.
[27] H. Torigoe, A. Maruyama, Synergistic stabilization of nucleic acid assembly by oligo-N3'->P5' phosphoramidate modification and additions of comb-type cationic copolymers, J. Am. Chem. Soc. 127 (2005) 1705–1710.
[28] H. Torigoe, K. Sasaki, T. Katayama, Thermodynamic and kinetic effects of morpholino modification on pyrimidine motif triplex nucleic acid formation under physiological condition, J. Biochem. 146 (2009) 173–183.
[29] H. Torigoe, A. Maruyama, S. Obika, T. Imanishi, T. Katayama, Synergistic stabilization of nucleic acid assembly by 2'-O,4'-C-methylene-bridged nucleic acid modification and additions of comb-type cationic copolymers, Biochemistry 48 (2009) 3545–3553.
[30] N. Langerman, R.L. Biltonen, Microcalorimeters for biological chemistry: applications, instrumentation and experimental design, Methods Enzymol. 61 (1979) 261–286.
[31] R.L. Biltonen, N. Langerman, Microcalorimetry for biological chemistry: experimental design, data analysis, and interpretation, Methods Enzymol. 61 (1979) 287–318.
[32] T. Wiseman, S. Williston, J.F. Brandts, L.N. Lin, Rapid measurement of binding constants and heats of binding using a new titration calorimeter, Anal. Biochem. 179 (1989) 131–137.
[33] H. Torigoe, R. Shimizume, A. Sarai, H. Shindo, Triplex formation of chemically modified homopyrimidine oligonucleotides: thermodynamic and kinetic studies, Biochemistry 38 (1999) 14653–14659.
[34] M. Rougee, B. Faucon, J.L. Mergny, F. Barcelo, C. Giovannangeli, T. Garestier, C. Helene, Kinetics and thermodynamics of triple-helix formation: effects of ionic strength and mismatches, Biochemistry 31 (1992) 9269–9278.
[35] L. Lavelle, J.R. Fresco, UV spectroscopic identification and thermodynamic analysis of protonated third strand deoxycytidine residues at neutrality in the triplex $d(C(+)\text{-}T)_6$:[$d(A\text{-}G)_6.d(C\text{-}T)_6$]; evidence for a proton switch, Nucleic Acids Res. 23 (1995) 2692–2705.
[36] G. Manzini, L.E. Xodo, D. Gasparotto, F. Quadrifoglio, G.A. van der Marel, J.H. van Boom, Triple helix formation by oligopurine-oligopyrimidine DNA fragments. Electrophoretic and thermodynamic behavior, J. Mol. Biol. 213 (1990) 833–843.
[37] K.H. Johnson, D.M. Gray, J.C. Sutherland, Vacuum UV CD spectra of homopolymer duplexes and triplexes containing A.T or A.U base pairs, Nucleic Acids Res. 19 (1991) 2275–2280.
[38] E. Wickstrom, Oligodeoxynucleotide stability in subcellular extracts and culture media, J. Biochem. Biophys. Methods 13 (1986) 97–102.
[39] H. Edelhoch, J.C. Osborne Jr., The thermodynamic basis of the stability of proteins, nucleic acids, and membranes, Adv. Protein Chem. 30 (1976) 183–250.
[40] Y.K. Cheng, B.M. Pettitt, Stabilities of double- and triple-strand helical nucleic acids, Prog. Biophys. Mol. Biol. 58 (1992) 225–257.
[41] M. Kamiya, H. Torigoe, H. Shindo, A. Sarai, Temperature dependence and sequence specificity of DNA triplex formation: an analysis using isothermal titration calorimetry, J. Am. Chem. Soc. 118 (1996) 4532–4538.
[42] R.H. Shafer, Stability and structure of model DNA triplexes and quadruplexes and their interactions with small ligands, Prog. Nucleic Acid Res. Mol. Biol. 59 (1998) 55–94.
[43] H. Fukada, K. Takahashi, Enthalpy and heat capacity changes for the proton dissociation of various buffer components in 0.1M potassium chloride, Proteins 33 (1998) 159–166.
[44] V. Tereshko, S. Gryaznov, M. Egli, Consequences of replacing the DNA 3'-oxygen by an amino group: high-resolution crystal structure of a fully

modified N3'->P5' phosphoramidate DNA dodecamer duplex, J. Am. Chem. Soc. 120 (1998) 269–283.
[45] D. Barsky, M.E. Colvin, G. Zon, S.M. Gryaznov, Hydration effects on the duplex stability of phosphoramidate DNA-RNA oligomers, Nucleic Acids Res. 25 (1997) 830–835.
[46] N.K. Banavali, A.D. MacKerell, Re-examination of the intrinsic, dynamic and hydration properties of phosphoramidate DNA, Nucleic Acids Res. 29 (2001) 3219–3230.
[47] G. Zon, T.G. Geiser, Phosphorothioate oligonucleotides: chemistry, purification, analysis, scale-up and future directions, Anticancer Drug Des 6 (1991) 539–568.
[48] C.A. Stein, J.L. Tonkinson, L. Yakubov, Phosphorothioate oligodeoxynucleotides–anti-sense inhibitors of gene expression? Pharmacol. Ther. 52 (1991) 365–384.
[49] L. Xodo, M. Alunni-Fabbroni, G. Manzini, F. Quadrifoglio, Pyrimidine phosphorothioate oligonucleotides form triple-stranded helices and promote transcription inhibition, Nucleic Acids Res. 22 (1994) 3322–3330.